TurboMeter: an attribution framework for ~~extreme~~ aviation turbulence events in a changing climate

Tommaso Alberti[1], Davide Faranda[2,3,4], Mohamed Foudad[5], Erika Coppola[6], Lia Rapella[4], Rachel Burbidge[7,8], Miguel A.C. Teixeira[9], and Paul Williams[5]

[1]Istituto Nazionale di Geofisica e Vulcanologia, via di Vigna Murata 605, 00143 Rome, Italy
[2]Laboratoire des Sciences du Climat et de l'Environnement, UMR 8212 CEA-CNRS-UVSQ, Université Paris-Saclay & IPSL, CE Saclay l'Orme des Merisiers, 91191, Gif-sur-Yvette, France
[3]London Mathematical Laboratory, 8 Margravine Gardens, London, W6 8RH, British Islands
[4]LMD-IPSL, Ecole Polytechnique, Institut Polytechnique de Paris, ENS, Université PSL, Sorbonne Université, CNRS, Palaiseau, France
[5]University of Reading, Whiteknights Road, Reading, UK
[6]International Centre for Theoretical Physics, Strada Costiera 11, Trieste, Italy
[7]Department of Natural Sciences, Manchester Metropolitan University, Manchester, United Kingdom
[8]EUROCONTROL, Brussels, Belgium
[9]IDMEC, Instituto Superior Tecnico, University of Lisbon, Lisbon, Portugal

Correspondence: Tommaso Alberti (tommaso.alberti@ingv.it)

Abstract.

Understanding the influence of climate change on aviation turbulence is critical for ensuring flight safety and developing adaptive strategies. Thus, we present TurboMeter, ~~an~~ a circulation-conditioned attribution framework that combines ~~reanalysis data with a conditional attribution methodology to assess whether the present-day atmosphere, under similar~~ objectively observed aircraft turbulence reports with atmospheric analogues to quantify how turbulence-favourable environments evolve under comparable large-scale synoptic ~~configurations, can lead to stronger aviation turbulence than in a cooler historical climate~~circulation conditions. Atmospheric analogues are identified using the complete 500-hPa geopotential height field (Z500), which constrains the large-scale circulation, while additional dynamical and thermodynamical diagnostics, i.e., upper-level wind speed, sea surface temperature (SST), 2-meter air temperature (T2m), total column water vapour (TCWV), Convective Available Potential Energy (CAPE), and Convective Inhibition (CIN), are subsequently analysed to provide a physical interpretation of the analogue populations. Turbulence diagnostics~~—~~, namely the Turbulence Index (TI1) and its two components, vertical wind shear and total deformation~~—~~, are used to characterize cruise-level moderate-or-greater (MOG) turbulence events reported ~~in~~ during 2024 ~~over four key flight~~ across four major aviation corridors: the North Atlantic, ~~the~~ North Pacific, East Asia, and the Contiguous United States (CONUS).

~~Our results highlight enhanced vertical~~ Under comparable synoptic conditions, present-day analogues consistently exhibit enhanced upper-level wind shear and ~~deformation in the present period, with increases ranging from 20% to 50% relative to historical analogues~~stronger turbulence diagnostics, together with warmer lower-boundary conditions and increased atmospheric moisture. The oceanic corridors (North Atlantic and North Pacific) are primarily characterized by coherent increases in SST, TCWV, upper-level wind speed, and vertical wind shear, whereas the continental regions (East Asia and CONUS) additionally

exhibit stronger thermodynamic responses, including localized increases in CAPE. Attribution diagnostics indicate that all events are at least partially influenced by anthropogenic climate change, with approximately 68% (2142 of 3123 reports) classified as being mainly strengthened by anthropogenic forcing, particularly over the North Atlantic, CONUS, and East Asia. A smaller but non-negligible share (about 32%) is associated with a combination of climate change and natural variability. In contrast, over the North Pacific, the majority of events (81%) fall into this latter category, highlighting a comparatively stronger role of internal climate variability in that region, consistent with previous studies showing a regionally dependent interplay between anthropogenic forcing and internal climate variability. These findings are further supported by the observed spatial patterns of increased turbulence-favourable conditions and suggest that anthropogenic climate change modifies not only the dynamical but also the thermodynamic environments in which aviation turbulence develops, although through regionally distinct physical pathways. These underscore the growing relevance of climate-informed diagnostics for aviation risk planning by considering both anthropogenic climate change and internal climate variability in projecting future turbulence risk.

1 Introduction

Aviation turbulence is a major concern for modern air travel, with important implications for aviation safety, passenger comfort, and operational efficiency (Sharman and Lane, 2016). Each year, turbulence causes numerous injuries, damages aircraft cabins, leads to flight delays and diversions, and increases fuel consumption due to avoidance maneuvers and longer flight paths (Burbidge et al., 2024). Recent advances in automated in situ turbulence observations based on the eddy dissipation rate (EDR) have substantially improved the objective characterization of aviation turbulence, enabling the construction of long-term climatologies and supporting both operational forecasting and climate studies (Sharman et al., 2014; Kim et al., 2020). Compared with traditional pilot reports (PIREPs), EDR is the standard ICAO metric for reporting aircraft turbulence intensity and it provides a quantitative and largely aircraft-independent measure of turbulence intensity, making it particularly suitable for climatological and attribution analyses (, ICAO).

While turbulence has always been an inherent part of atmospheric flight, recent studies suggest that its frequency and intensity—particularly that of ~~clear air~~ clear-air turbulence (CAT)—may be increasing over time (Williams, 2017; Storer et al., 2019; Alberti et al., 2024; Foudad et al., 2024; Lee et al., 2023; Prosser et al., 2023; Jaeger and Sprenger, 2007). Unlike turbulence associated with convective storms or clouds over mountainous terrain (Lane et al., 2012; Guarino et al., 2018), CAT occurs in clear skies, often at cruising altitudes, making it difficult to detect and avoid using conventional radar systems (Dutton, 1971; Foudad et al., 2024). Nevertheless, aviation turbulence is intrinsically a multiscale phenomenon. Although clear-air turbulence frequently develops in association with upper-level jets and strong vertical shear, turbulence may also result from mountain-wave breaking, convectively induced gravity waves, frontal circulations, tropical-cyclone outflow, and other mesoscale dynamical processes (Kim and Chun, 2010, 2012; Kim et al., 2014; Trier et al., 2020; Kim et al., 2021; Baek et al., 2024; Lee e . The relative contribution of these mechanisms varies considerably among regions and individual events, making the attribution of observed turbulence particularly challenging.

The prospect that climate change may be intensifying ~~turbulence has become a critical~~ aviation turbulence has therefore become an active area of scientific investigation (Williams and Joshi, 2013; Storer et al., 2017; Gratton et al., 2022). As global temperatures rise due to anthropogenic greenhouse gas emissions, the structure and dynamics of the atmosphere are undergoing substantial changes. In particular, the upper troposphere and lower stratosphere (UTLS), ~~the region~~ where most commercial aircraft operate (Sharman and Lane, 2016), has ~~seen increases~~ experienced changes in wind shear and meridional temperature gradients, especially over East Asia (Lee et al., 2023), two of the ~~main drivers of turbulence that are related via thermal wind balance. The~~ primary dynamical ingredients controlling upper-level turbulence through the thermal wind relationship. Simultaneously, the warming of the troposphere and the cooling of the stratosphere, both ~~fingerprint effects of~~ well-established fingerprints of anthropogenic climate change, are expected to ~~strengthen the polar~~ modify the strength and structure of the upper-level jet streams (Shaw and Miyawaki, 2023)~~and increase the likelihood of instabilities that trigger CAT~~, thereby influencing the atmospheric environments favourable to turbulence development (Smith et al., 2023).

Previous ~~modeling~~ modelling studies (Williams and Joshi, 2013; Williams, 2017) have projected a significant increase in moderate-to-severe turbulence ~~in~~ over major flight corridors ~~across the North Atlantic~~ by the end of the century under ~~high-emissions~~ high-emission scenarios. However, ~~quantifying~~ determining whether such changes are already detectable in ~~observational data~~present-day observations—and ~~how much of that change can be attributed to anthropogenic climate forcing~~quantifying the respective contributions of anthropogenic climate change and natural atmospheric variability—~~requires a robust attribution framework~~ remains considerably more challenging (Alberti et al., 2024; Rapella et al., 2025). This ~~task is challenging~~ difficulty arises because turbulence is a localized and ~~transient phenomenon that is difficult to observe directly. Therefore, studies often~~ intermittent phenomenon whose generation depends on interactions across multiple spatial scales. Consequently, long-term analyses generally rely on reanalysis datasets ~~and turbulence proxies~~together with turbulence diagnostics, such as the Ellrod indices (Ellrod and Knapp, 1992; Ellrod and Knox, 2010), ~~to study long-term trends~~ rather than on direct observations alone (Prosser et al., 2023; Jaeger and Sprenger, 2007; Foudad et al., 2024).

~~This paper aims to detect the influence of climate change on aviation-relevant turbulence by proposing a novel conditional attribution framework:~~ In this study, we introduce *TurboMeter*~~building on~~, a conditional analogue-based attribution framework that builds upon the rapid-attribution ~~framework ClimaMeter (Faranda et al., 2024), developed by a consortium of scientists and research institutes to understand extreme weather events in a changing climate based on looking at similar past weather situations. In this way, we assess whether the atmosphere, under similar~~ methodology developed within ClimaMeter (Faranda et al., 2024). Rather than attempting to identify the specific physical mechanism responsible for each turbulence encounter, TurboMeter constrains the large-scale ~~synoptic conditions, is more conducive to turbulence today than in a cooler historical climate. TurboMeter thus provides a practical and~~ atmospheric circulation through atmospheric analogues and subsequently evaluates whether turbulence-relevant atmospheric diagnostics differ between historical and present-day climates under comparable synoptic conditions. This circulation-conditioned approach provides a physically interpretable framework ~~to quantify the changes in aviation turbulence in a warming climate—information that is directly relevant to aviation safety, flight route planning, and climate adaptation strategies~~for separating changes associated with large-scale atmospheric variability from those emerging under different climatic backgrounds.

We assess ~~our~~ the framework using 3123 upper-level (≥≥8 km) moderate-or-greater turbulence ~~episodes observed across four key flight corridors, i.e.,~~ reports corresponding to 31 turbulence days observed during 2024 across four major flight corridors: the North Atlantic, North Pacific, East Asia, and ~~CONUS during 31 days of 2024. The 200-250 hPa pressure level (existing at approximately 10-12 kmaltitude), this pressure level typically lies near the tropopause, the boundary separating the upper troposphere from the lower stratosphere. It plays a key role in large-scale atmospheric dynamics and~~ the continental United States (CONUS). The attribution analysis focuses on the 200–250 hPa layer, corresponding approximately to cruising altitudes (10–12 km), where commercial aircraft operate and where turbulence is closely associated with ~~the core of the jet streams. In the following, we provide evidence of the accuracy of our framework for four selected days over each region~~upper-level jet dynamics. Additional diagnostics of upper-level winds, total column water vapour (TCWV), convective available potential energy (CAPE), and convective inhibition (CIN) are incorporated to provide an additional physical assessment of the selected analogues and to strengthen the interpretation of the attribution results. Representative case studies for each flight corridor are discussed in the main text, while the ~~full set of events is reported~~ complete set of analysed events is provided in the Supplementary ~~Materials~~Material.

2 Data & Methods

2.1 Data

~~This study uses data from ERA5,~~

This study combines objective in situ aircraft turbulence observations with atmospheric fields from the ERA5 reanalysis. Turbulence events are identified from automated eddy dissipation rate (EDR) reports, while ERA5 is used both to characterize the large-scale atmospheric circulation associated with each event and to evaluate the corresponding turbulence-relevant atmospheric diagnostics.

ERA5 is the fifth-generation global atmospheric reanalysis produced by the European Centre for Medium-Range Weather Forecasts (ECMWF). ERA5 ~~offers a detailed,~~ provides a physically consistent reconstruction of the global ~~climate at an~~ atmosphere with hourly temporal resolution and approximately 31 km horizontal resolution, covering the period from 1950 to the present (Hersbach et al., 2020). ~~It is widely used in climate and weather research and is especially suitable for studies requiring long-term, high-resolution atmospheric fields.~~ Owing to its temporal consistency and comprehensive representation of the atmospheric state, ERA5 has become one of the standard datasets for climatological analyses and analogue-based attribution studies.

Observed turbulence events are identified using automated in situ aircraft reports based on the eddy dissipation rate (EDR), which provides an objective and largely aircraft-independent measure of turbulence intensity (Sharman et al., 2014; Kim et al., 2020) and it is the standard ICAO metric for reporting aircraft turbulence intensity (, ICAO). Unlike traditional pilot reports (PIREPs), EDR offers a quantitative estimate of turbulence that is largely independent of aircraft type and operational conditions, making it particularly suitable for climatological analyses. Following operational practice, this study focuses on moderate-or-greater

turbulence reports (EDR $\geq 0.2\ \mathrm{m}^{2/3}\ \mathrm{s}^{-1}$). This threshold is used exclusively to identify objectively observed turbulence events and should not be interpreted as an operational definition of "extreme" turbulence.

To investigate ~~trends~~ changes in aviation-relevant ~~turbulence~~ atmospheric environments and assess the ~~potential~~ influence of climate change, we ~~extract and analyze the following key~~ analyse the following atmospheric variables:

- ~~**500 hPa**~~ **500-hPa geopotential height (Z500):** used ~~to characterize the~~ exclusively to identify circulation analogues by characterizing the large-scale atmospheric circulation associated with each event. Z500 provides a robust description of synoptic-scale ~~patterns and identify the presence of systems (e.g., cyclones, anticyclones,~~ weather systems, including ridges, troughs, cut-off lows~~) that can influence~~ , cyclones and anticyclones, which control the upper-level ~~jet dynamics and turbulence generation.~~ dynamical environment.

- **Vertical Wind Shear (VWS):** quantifies wind variations with ~~the height~~z~~,~~ height,

$$\mathrm{VWS} = \sqrt{\left(\frac{\partial u}{\partial z}\right)^2 + \left(\frac{\partial v}{\partial z}\right)^2}\sqrt{\left(\frac{\partial u}{\partial z}\right)^2 + \left(\frac{\partial v}{\partial z}\right)^2}, \tag{1}$$

~~where (u) and (v) are~~

where u and v denote the zonal and meridional wind components, respectively, and ~~(z) denotes~~ z is the vertical coordinate~~, and it~~ . VWS provides a measure of ~~shear instability , which can trigger CAT.~~ dynamical instability that is closely associated with clear-air turbulence.

- **Total Deformation (DEF):** ~~represents the distortion of air parcels due to~~ describes the horizontal stretching and shearing ~~and it is related to increased frontogenesis,~~ deformation of the flow,

$$\mathrm{DEF} = \sqrt{\left(\frac{\partial u}{\partial x} - \frac{\partial v}{\partial y}\right)^2 + \left(\frac{\partial v}{\partial x} + \frac{\partial u}{\partial y}\right)^2}\sqrt{\left(\frac{\partial u}{\partial x} - \frac{\partial v}{\partial y}\right)^2 + \left(\frac{\partial v}{\partial x} + \frac{\partial u}{\partial y}\right)^2}, \tag{2}$$

~~where (x) and (y) represent~~

where x and y are the horizontal coordinates.

- **Ellrod Turbulence Index (TI1):** ~~provides a diagnostic measure of CAT potential as the product of the horizontal wind deformation and vertical wind shear (Ellrod and Knapp, 1992),~~

$$\mathrm{TI1} = \mathrm{VWS} \times \mathrm{DEF}$$

combines vertical wind shear and horizontal deformation into a diagnostic proxy for upper-level turbulence potential (Ellrod and Knapp, 1992),

$$TI1 = VWS \times DEF. \quad (3)$$

– **Upper-level wind speed (250 hPa), total column water vapour (TCWV), convective available potential energy (CAPE), convective inhibition (CIN), 2-meter temperature (t2m) and sea surface temperature (SST):** these variables are not used during the analogue-selection procedure but are analysed a posteriori to provide an additional physical assessment of the selected analogues and to support the interpretation of the attribution results.

Throughout the analysis, Z500 is used exclusively to identify circulation analogues, whereas the remaining atmospheric variables are evaluated only after analogue selection. Furthermore, VWS, DEF and TI1 are calculated around 250hPa being representative of commercial flights cruise altitude. ERA5 ensures spatial and temporal consistency across decades, making it possible to identify robust ~~trends and perform~~ circulation analogues and perform circulation-conditioned attribution analyses (Faranda et al., 2023; Alberti et al., 2024).

2.2 Conditional analogue-based attribution

To evaluate whether observed changes in turbulence metrics are linked to anthropogenic climate change, we implement an analogue-based attribution ~~method, based on the ClimaMeter framework~~ framework based on ClimaMeter (Yiou et al., 2017; Faranda et al., 2024). This approach ~~uses historical~~ identifies atmospheric analogues to isolate the ~~influence~~ contribution of climate change ~~on~~ while conditioning the analysis on comparable large-scale circulation patterns (Jézéquel et al., 2018; Faranda et al., 2023 . Rather than attempting to reproduce the complete atmospheric state associated with each turbulence encounter, TurboMeter constrains the synoptic-scale circulation and subsequently evaluates whether turbulence-relevant atmospheric diagnostics differ between historical and present-day ~~atmospheric phenomena (Jézéquel et al., 2018; Faranda et al., 2023). It~~ climates under comparable circulation conditions. The framework consists of the following steps:

1. **Event Selection:** ~~we begin by identifying turbulence-prone days~~ Turbulence-prone days are identified using automated in situ reports from commercial aircraft, obtained from the Meteorological Assimilation Data Ingest System (MADIS) archive maintained by the National Oceanic and Atmospheric Administration (NOAA). These reports are based on the Aircraft Communications Addressing and Reporting System (ACARS) and provide estimates of the cubic root of the eddy dissipation rate (EDR). EDR provides an objective and aircraft-independent measure of turbulence intensity and is the standard metric adopted operationally in aviation ~~(?)~~(Sharman et al., 2014). We retain only quality-controlled reports above 8 km altitude. Full details of the dataset and preprocessing are given in ~~Kaluza et al. (2026).~~ Kaluza et al. (2026). Here, we focus on days in 2024 for which EDR $\geq\geq$ 0.2 $m^{2/3}$ s^{-1}, corresponding to moderate-or-greater (MOG) turbulence events, over four domains: North Atlantic (643 reports), North Pacific (425), East Asia (150), and CONUS (1905)[1]. The event definition is intentionally observation-based rather than process-based. Consequently, no distinction is

[1] ~~We need to underline that the~~ The turbulence dataset from NOAA MADIS ~~reports~~ is dominated by U.S. airlines, with more than 50% of ~~events~~ reports occurring over CONUS, ~~while~~ whereas East Asia is represented by only about 150 ~~events~~reports. ~~As a result~~Consequently, conclusions for East Asia should

made between clear-air turbulence, mountain-wave turbulence, convectively induced turbulence, or other turbulence-generation mechanisms. These processes are instead discussed a posteriori through additional atmospheric diagnostics.

2. **Analogue Identification:** ~~for each day~~ For each event day, we search for historical (~~1950-2023~~1950–2023) analogue days ~~that share similar 500 hPa geopotential height~~ sharing similar 500-hPa geopotential height (Z500) patterns over the ~~analyzed domain and over~~ analysed domain and within the same season~~when the event occurred~~. The 500-hPa geopotential height field is used because it provides a robust representation of the synoptic-scale atmospheric circulation controlling the upper-level dynamical environment in which aviation turbulence develops. Analogues are ~~chosen~~ identified as the top 1% ~~maps~~ of circulation patterns minimizing the Euclidean distance between the event Z500 field ~~of the event and the remaining~~ and all candidate Z500 fields in the ~~database (Faranda et al., 2024).~~ ERA5 archive (Faranda et al., 2024) . It is important to emphasize that similarity in Z500 does not imply identical turbulence-generation mechanisms or identical atmospheric states. Instead, it identifies comparable large-scale circulation configurations suitable for circulation-conditione attribution.

3. **Climate Attribution:** ~~once analogues are established~~Once the analogues have been identified, we compare the distributions of turbulence-related ~~indicators, i.e.~~diagnostics, e.g., TI1~~and its two components (VWS and DEF)~~ , between the present climate (~~1987-2023~~1987–2023) and the ~~past climate (1950-1986)~~historical climate (1950–1986)[2]. An increase in turbulence ~~metrics in the recent analogues, despite similar synoptic-scale structures, suggests a climate change fingerprint.~~ diagnostics within the present-day analogue population, despite comparable large-scale circulation, is interpreted as evidence of a climate-change fingerprint. Additional atmospheric diagnostics, including upper-level wind speed at 250 hPa, total column water vapour (TCWV), convective available potential energy (CAPE), convective inhibition (CIN), 2-meter temperature (t2m), and sea surface temperature (SST) are also analysed independently of the analogue-selection procedure to support the physical interpretation. Statistical significance in the differences between the two periods is assessed at each grid point using bootstrap resampling (Faranda et al., 2024) from repeated resamples of the analogue pool by selecting the 95% as significance level.

4. **Assessment:** ~~results~~ Results are expressed in terms of likelihoods, such as ~~"~~"a 30% increase in TI1 values due to ~~human-induced climate change".~~ climate change".

5. **Visual summary:** ~~we provide a simple and intuitive visual way to interpret all diagnostic information related to the event under study~~ Results are summarized using the same graphical framework adopted by ClimaMeter through two gauge charts: the attribution gauge (left-hand gauge) and the rarity gauge (right-hand gauge). In the revised version of the manuscript, these diagnostics are complemented by additional dynamical and thermodynamical analyses that provide an additional physical assessment of the selected analogues and support the interpretation of the attribution results.

---

be regarded as ~~provisional, highlighting the need for improved regional~~ preliminary and ~~seasonal sampling in~~ motivate future ~~work~~analyses based on more regionally balanced datasets.

[2] ~~Considering~~ Following the standard ClimaMeter methodology (Faranda et al., 2024), the ERA5 ~~climatology up to 2024 we~~ record is divided ~~the full historical period~~ into two equal-length ~~ones as usual in attribution studies (Faranda et al., 2024)~~climatological periods.

The attribution gauge indicates the relative influence of natural climate variability versus climate change on the event, providing information on whether the event was strengthened by climate change or influenced by natural variability. This attribution is based on the differences in the distribution of three major modes of climate variability between the past and present periods as in Faranda et al. (2024): El Niño–Southern Oscillation (ENSO), Atlantic Multidecadal Oscillation (AMO), and Pacific Decadal Oscillation (PDO). Firstly, the statistical significance of the difference in phase distributions between the two periods is assessed by using a two-tailed von Mises test as in Faranda et al. (2024). Then, by considering each mode as equally contributing, we assign a 1/3 weight to each mode such that the possible gauge positions are (Faranda et al., 2024):

- pointing to the right: no significant differences across ENSO, AMO, or PDO, i.e., there is no influence of natural variability;
- pointing 2/3 to the right: one mode shows a significant difference;
- pointing 1/3 to the left: two modes show significant differences;
- pointing to the left: all three modes show significant differences.

The rarity gauge quantifies the *rarity* of the event's synoptic pattern. This is assessed using the analogue quality metric Q, as defined in Faranda et al. (2024), which measures the mean Euclidean distance between the event and its best analogues. To contextualize this value, Q is compared to a reference distribution Q_a, representing the Euclidean distances between the best analogues of the analogues of the event. The gauge position is determined as follows:

- pointing to the left: for both the past and present periods, $Q < P_{75}(Q_a)$, that is similar events have occurred in the past.
- pointing 1/3 to the left: for both periods, $P_{75}(Q_a) \leq Q < P_{95}(Q_a)$, that is moderately rare event.
- pointing 2/3 to the right: Q exceeds $P_{95}(Q_a)$ in one period and lies between $P_{75}(Q_a)$ and $P_{95}(Q_a)$ in the other, that is increasingly quite exceptional.
- pointing to the right: $Q > P_{95}(Q_a)$ in both periods, that is the event is very exceptional within the data record.

High percentiles are used to determine gauge thresholds since the analysis focuses on ~~extreme~~ rare events, which are, by definition, rarely observed.

In both gauges, the needle can take four discrete positions serving as ordinal categories reflecting increasing confidence in the attribution or rarity assessment. These values, designed as visual indicators to convey complex diagnostic outcomes in an intuitive way, are also used to classify the event in the following categories as in Faranda et al. (2024):

- **strengthened by human-driven climate change:** both gauge indicators are on red;
- **mostly strengthened by human-driven climate change:** one of the gauge indicators is on red and the other is on gray/orange;

- **likely influenced by both human-driven climate change and natural variability:** both gauge indicators are on gray/orange or one is on green/yellow and one on gray/orange;
- **mostly driven by natural variability:** ~~both~~ the left gauge indicator is on green and the right gauge is on yellow;
- **low confidence:** if the attribution gauge indicator is on green and the rarity gauge indicator is on red.

This method, as its original source-based ClimaMeter (Faranda et al., 2024), offers a physically interpretable, observationally grounded alternative to model-only attribution studies. It allows us to evaluate whether the atmosphere, under similar synoptic configurations, is now more prone to producing turbulence than it was decades ago. To display the results we use the same format of ClimaMeter thus presenting in the first ~~raw~~ row the attribution gauges, the second ~~raw~~ row shows the meteorological and turbulence conditions during the event of interest, the third ~~raw~~ row reports the differences between the present and the past, while the bottom ~~raw~~ row reports the changes in the monthly occurrence in the two periods and the changes observed over airports. Since our events are all upper-level ones, we cannot detect changes at airports' level. However, we decided to ~~mantain~~ maintain the structure to provide a more general format that can be used also to assess changes at low levels in future works.

3 Results

We present detailed case studies over the four regions to provide a comprehensive overview of the methodology, focusing on representative days with a large number of reported events. The full set of events for each region is shown in the Supplementary Material.

3.1 North Atlantic

The North Atlantic represents one of the busiest flight corridors worldwide and is characterized by strong baroclinicity and a persistent upper-level jet stream, making it particularly prone to clear-air turbulence. For the North Atlantic region, 643 MOG turbulence ~~events~~ reports (EDR ~~≥~~≥ 0.2 $m^{2/3}$ s^{-1}) from the NOAA MADIS archive were recorded ~~in~~ during 2024, with 25 February 2024 corresponding to the day with the highest number of ~~events~~ reports (88). As shown in ~~Figure~~Fig. 1, 89% (78/88) of the ~~events are located~~ reports are concentrated over the western North Atlantic, primarily ~~near the eastern US coast and extending northward to New York State~~along the eastern coast of North America and extending northeastward towards Newfoundland and the Labrador Sea.

~~Analogue-based results for the day 2024-02-25 over the North Atlantic region. Panels show (a) 500 hPa geopotential height anomalies, (b) the Ellrod index TI1, (c) the vertical wind shear (VWS), and (d) the horizontal deformation (DEF) during the event, and corresponding climate change signals present minus past (panels (e), (f), (g), and (h), respectively). Panels (i) and (j) represent the monthly distribution in the two periods and the changes observed in nearby airports if present. The dials above indicate attribution categories: influence of climate change (left) and statistical rarity (right) of the atmospheric meteorological configuration.~~

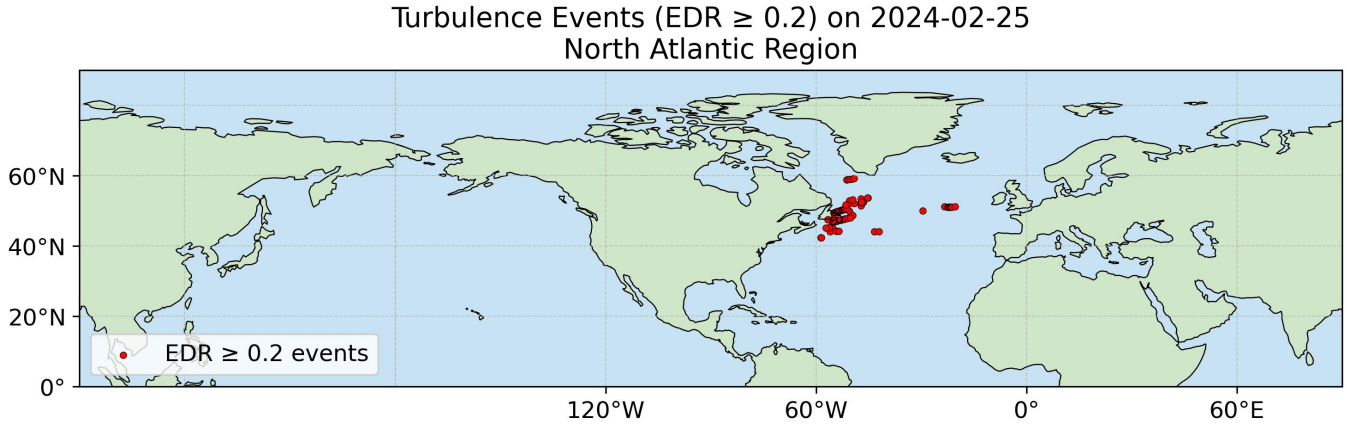


Figure 1. Distribution of ~~the~~ moderate-or-greater (MOG) turbulence ~~events~~ reports (EDR ~~≥~~ > 0.2 $m^{2/3}$ s^{-1}) from the NOAA MADIS archive on ~~2024-02-25~~ 25 February 2024 over the North Atlantic region.

The ~~meteorological conditions during the 2024-02-25 reveal a pronounced synoptic-scale pattern (Figure ??(a)), consistent with a strong~~ circulation-conditioned attribution analysis for this event is summarized in Fig. 2. The observed atmospheric configuration is characterized by a pronounced upper-level ~~trough–ridge configuration over the North Atlantic. This large-scale circulation supports an intense jet-stream structure, as evidenced by the Turbulence Index TI1 (Figure ??(b)), which exhibits localized maxima along the jet core, also corresponding to the geographical region where more events are reported (Figure 1~~ridge extending across the central North Atlantic (Fig. 2a), associated with a broad jet stream exceeding 50 m s^{-1} (Fig. 2b). Enhanced vertical wind shear ~~(Figure ??(c)) and strong horizontal deformation (Figure ??(d)) are co-located with these regions, indicating dynamically active flow and favorable conditions for the generation of clear air turbulence, particularly in association with jet streaks and sharp horizontal velocity gradients. In this region, strong vertical wind shear promotes shear-driven instabilities, while enhanced horizontal deformation is indicative of frontogenetic processes and the sharpening of horizontal velocity gradients. Their spatial co-location highlights the combined role of shear and strain in fostering favorable conditions for clear air turbulence , particularly in jet exit regions and downstream of upper-level troughs.~~develops along the southern flank of the jet (Fig. 2c), producing elevated values of the Ellrod turbulence index (TI1; Fig. 2d) over the central and eastern portions of the basin, in good agreement with the spatial distribution of the observed turbulence reports (Fig. 1).

~~By examining the differences between the present and the past period we highlight a coherent~~

The historical and present-day analogues reproduce highly comparable synoptic-scale circulation patterns, as evidenced by the relatively small differences in the Z500 field (Fig. 2e), although not statistically significant over almost all the domain. This indicates that the analogue-selection procedure successfully constrains the large-scale ~~anomaly pattern (Figure ??(e)), mostly located on the jet stream track, while percentage differences in TI1 (Figure ??(f)),~~ circulation associated with the observed event and that changes in synoptic-scale patterns are not statistically different. In contrast, the upper-level jet exhibits a moderate strengthening over portions of the eastern North Atlantic and south of Iceland (Fig. 2f), accompanied by coherent

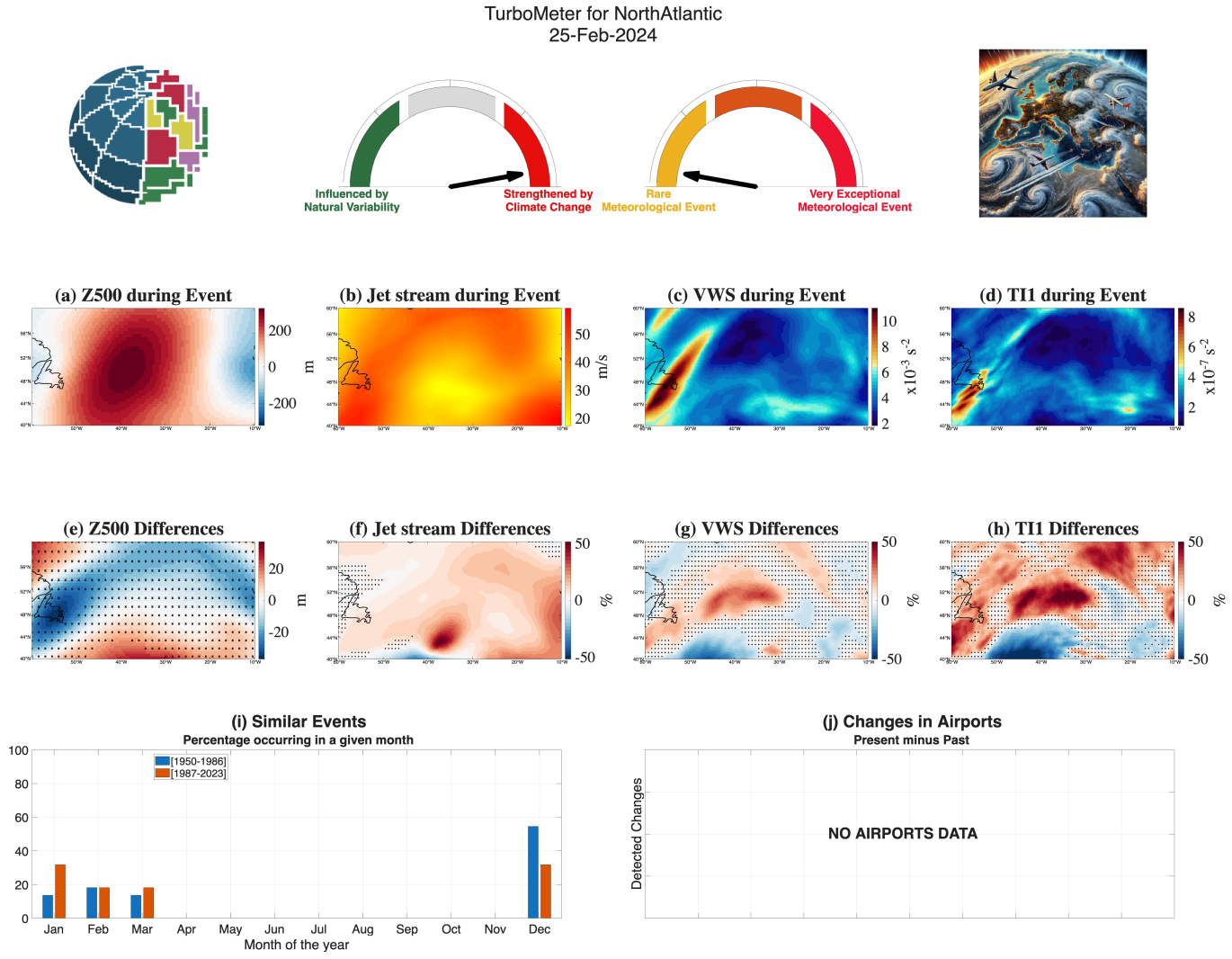


Figure 2. TurboMeter analysis for the North Atlantic turbulence event on 25 February 2024. Panels (a–d) show the observed atmospheric conditions during the event, whereas panels (e–h) present the circulation-conditioned differences between the historical (1950–1986) and present-day (1987–2023) analogues. Panel (i) shows the monthly distribution of analogue occurrence for the two climate periods, while panel (j) summarizes the changes in near-surface atmospheric variables over the available airports. Black stippling denotes regions where the differences are not statistically significant at the 95% confidence level.

increases in vertical wind shear (~~Figure ??(g)), and deformation (Figure ??(h)) show positive anomalies in the region where more events are reported (Figure 1). These differences indicate a substantial intensification of turbulence-relevant dynamical ingredients during the present compared to typical past conditions, especially along the main North Atlantic flight corridor. Figure ??(i)summarizes the seasonal distribution of similar historical events, expressed as the percentage of occurrences in~~

each month, comparing the past period (1950–1986) with the more recent one (1987–2023).The distribution suggest a shifts from Decemberto January in their seasonal occurrence, with relatively higher frequencies in early winter in the more recent period. Finally, the gauge indicators at the top of Figure **??** classify the 25 February 2024 eventas strongly intensified, with a substantial climate-change contribution, and as a rare meteorological eventFig. 2g).

In more detail, we observe that the composite fields for the past period (Figure **??**, panels a, c, e) depict a smoother and strongly curved storm-track structure.Maxima of These dynamical changes translate into a pronounced enhancement of TI1 , VWS, andDEF are confined to a relatively narrow jet corridor, consistent with a classical baroclinic regime dominated by synoptic-scale variability and moderate over the central North Atlantic (Fig. 2h), with the close spatial correspondence between VWS and TI1 indicating that the strengthened turbulence-favourable environment is primarily associated with enhanced upper-level shear. This configuration reflects a background state in which turbulence generation is primarily episodic and tightly linked to individual cyclones.shear rather than changes in horizontal deformation.

The attribution gauge indicates that the event was predominantly strengthened by climate change, whereas the rarity gauge suggests that similar synoptic configurations remain characteristic of the winter season in both climatological periods. This interpretation is further supported by the seasonal distribution of the analogues (Fig. 2i), which remains concentrated during December, January and February in both climate periods, indicating that the comparison is performed under similar seasonal circulation regimes. Although airport-scale diagnostics (Fig. 2j) are of limited relevance for this upper-level event, they are retained to preserve the standard TurboMeter visualization and facilitate future applications to lower-tropospheric hazards.

To further investigate the physical environment associated with the selected analogues, Figs. 3 and 4 present complementary diagnostics that are independent of the analogue-selection procedure.

The additional surface diagnostics reveal that the historical and present-day analogues retain highly comparable synoptic-scale circulation patterns, as confirmed by the limited (and not significant) differences in Z500 (Fig. 3d). In contrast, the composites for the recent period (Figure **??**, panels b, d, f)reveal an intensification and spatial broadening of all three fields along the jet axis. Enhanced VWS suggests a strengthening of upper-tropospheric wind gradients, while increased DEF indicates more frequent or more intense deformation-driven flow configurationssea surface temperatures exhibit widespread positive anomalies across much of the North Atlantic (Fig. 3h), particularly along the Gulf Stream extension and toward the Labrador Sea, where warming locally exceeds 1–2 °C. Surface wind speed also displays moderate positive anomalies over the central North Atlantic (Fig. 3l), suggesting a slightly more energetic lower-tropospheric environment under present-day climate conditions. Together, these features point to a modified jet-stream structure that is dynamically more conducive to turbulence generation even outside the most extreme synoptic events. changes indicate that the analogues evolve over a systematically warmer ocean while maintaining nearly identical large-scale circulation.

The surface warming is reflected in the thermodynamic environment (Fig. 4). CAPE remains generally low throughout the basin (Fig. 4a–d), while CIN exhibits only weak and spatially fragmented differences between the two analogues (Fig. 4e–h), indicating that large-scale convective instability plays only a secondary role for this event. In contrast, total column water vapour displays a coherent increase across the central and western North Atlantic (Fig. 4l), consistent with the warmer and moister atmospheric background expected under present-day climate conditions. These suggest that analogues develop within

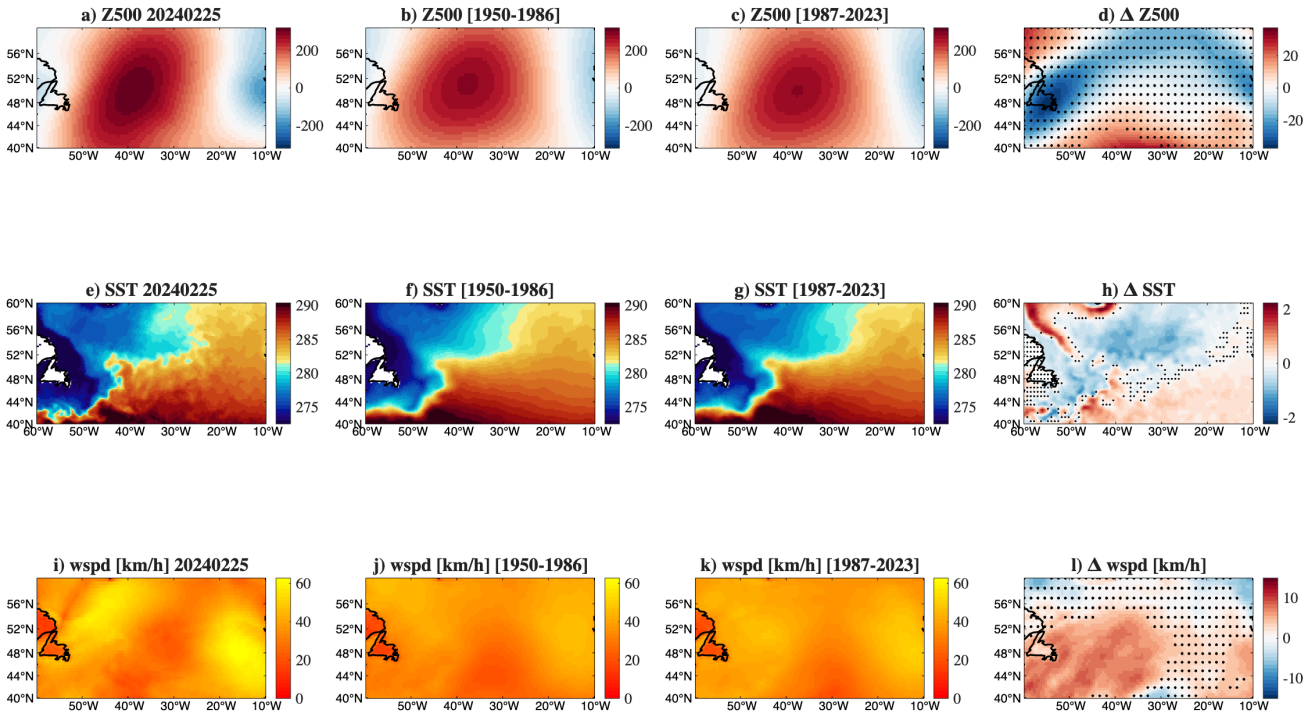


Figure 3. Additional atmospheric and surface diagnostics for the North Atlantic analogues. Panels (a–d) show the 500-hPa geopotential height (Z500) for the observed event, the historical analogue composite (1950–1986), the present-day analogue composite (1987–2023), and the corresponding present-minus-past differences. Panels (e–h) show the same for Sea Surface Temperature (SST), while panels (i–l) for 10-m surface wind speed. Black stippling denotes regions where the differences are not statistically significant at the 95% confidence level.

a systematically moister atmosphere that can favor convection and then upper-level turbulence. These thermodynamic changes are indeed accompanied by enhanced upper-level wind shear (Fig. 2g), ultimately producing larger TI1 values (Fig. 2h).

By considering all the 643 MOG turbulence reports (EDR ≥ 0.2 $m^{2/3}$ s^{-1}) in the North Atlantic region occurred in 2024 (see Supplementary Materials) we observe that the meteorological conditions in around 8% (51 over 643) of events have been strengthened by human-driven climate change, 71% (457 over 643) have been mostly strengthened by human-driven climate change, and the remaining 21% (135 over 643) have been likely influenced by both human-driven climate change and natural variability. We do not detect any event only driven by natural variability and for all events we have medium-to-high confidence in our claims.

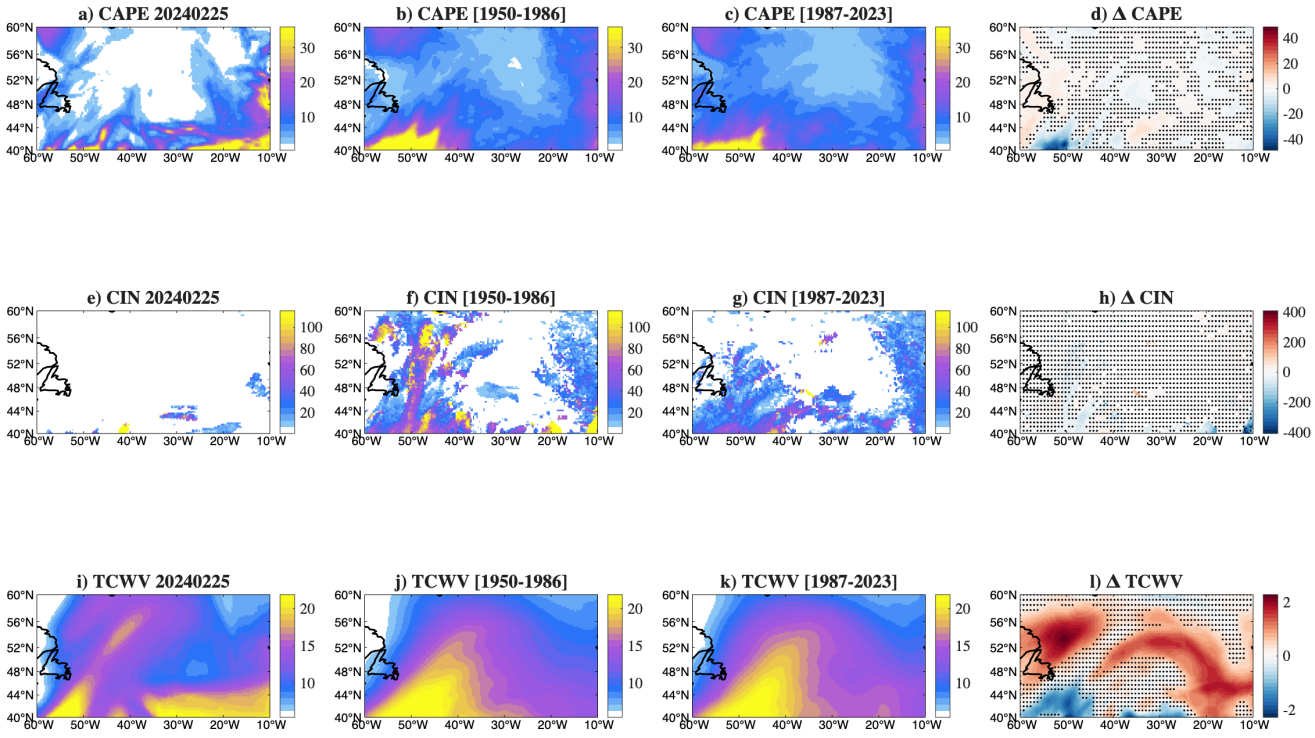


Figure 4. ~~Analogue-based results~~ Additional thermodynamical diagnostics for the ~~day 2024-02-25 over the~~ North Atlantic ~~region~~analogues. ~~a) composite TI1 during the past period~~ Panels (~~1950–1986~~a–d) ~~, b) composite TI1 during~~ show the ~~present period~~ Convective Available Potential Energy (~~1987–2023~~CAPE) for the observed event, ~~c) composite VWS during~~ the ~~past period~~ historical analogue composite (1950–1986), ~~d) composite VWS during~~ the ~~present period~~ present-day analogue composite (1987–2023), ~~e~~and the corresponding present-minus-past differences. Panels (e–h) ~~composite DEF during~~ show the ~~past period~~ same for Convective Inhibition (~~1950–1986~~CIN), ~~f~~while panels (i–l) ~~composite DEF during the present period~~ for Total Column Water Vapour (~~1987–2023~~TCWV). Black stippling denotes regions where the differences are not statistically significant at the 95% confidence level.

3.2 North Pacific

The North Pacific constitutes one of the most dynamically active aviation corridors, where intense upper-level jet streams, strong baroclinicity, and frequent cyclonic activity create favourable conditions for aviation turbulence throughout the cold season. For the North Pacific region, 425 MOG turbulence ~~events~~ reports (EDR ~~≥~~≥ 0.2 $m^{2/3}$ s^{-1}) from the NOAA MADIS archive were recorded ~~in~~ during 2024, with 20 December 2024 corresponding to the day with the highest number of ~~events~~ reports (104). ~~Examination of the spatial distribution of the reports (Figure 5) reveals~~ As shown in Fig. 5, the observed

turbulence reports are organized into two distinct clustersof events: a smaller cluster located north of 40°N and closer to the coast : a northern cluster located close to the west coast of North America (27%, 28/104) , and a larger cluster located south of 40°N subtropical cluster extending across the central North Pacific (73%, 76/104), reflecting the broad-scale structure of the upper-level jet.

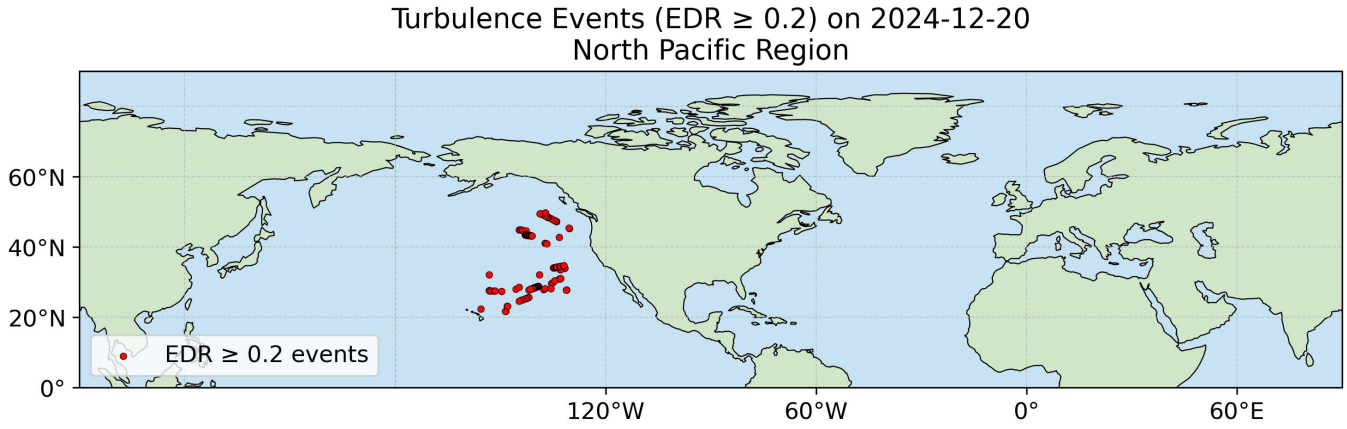


Figure 5. Distribution of the moderate-or-greater (MOG) turbulence events reports (EDR ≥≥ 0.2 $m^{2/3}$ s^{-1}) from the NOAA MADIS archive on 2024-12-20 20 December 2024 over the North Pacific region.

The meteorological conditions during 2024-12-20 display a pronounced negative pattern over the circulation-conditioned attribution analysis for this event is summarized in Fig. 6. The observed atmospheric configuration is characterized by a deep upper-level trough over the central North Pacific (Figure **??**(a)), corresponding to intensified cyclogenesis and an active storm track, resembling the typical winter El Nino pattern. These patterns are also characteristic of dynamically active wintertime flow associated with frequent baroclinic wave development, with enhanced deformation concentrated within jet streak entrance and exit regions along the Pacific storm track, where horizontal deformation is strongest. Therefore, it favors the development of shear-driven instabilities linked to clear air turbulence (CAT) at typical cruise altitudes.Indeed, in the same region TI1 shows large values (Figure **??**(b)), mostly due to increases in the Fig. 6a), associated with a broad jet stream exceeding 70 m s^{-1} (Fig. 6b). Enhanced vertical wind shear (Figure **??**(c)) over a wide area corresponding to the depression. Additionally, also the horizontal deformation presents large values (Figure **??**(d)), particularly in the core of the cyclonic anomaly.develops along the southern flank of the jet (Fig. 6c), producing a broad region of elevated TI1 values (Fig. 6d) matching the spatial distribution of the observed turbulence reports (Fig. 5).

The differences between the present and the past period suggest that similar atmospheric configurations are now deeper (-20 m), highlighting a coherent

The historical and present-day analogues reproduce remarkably similar synoptic-scale circulation patterns, with relatively weak differences in Z500 (Fig. 6e), again confirming that the analogue-selection procedure successfully constrains the large-scale anomaly pattern (Figure **??**(e)), associated with increases in the present conditions of all turbulence-related metrics.

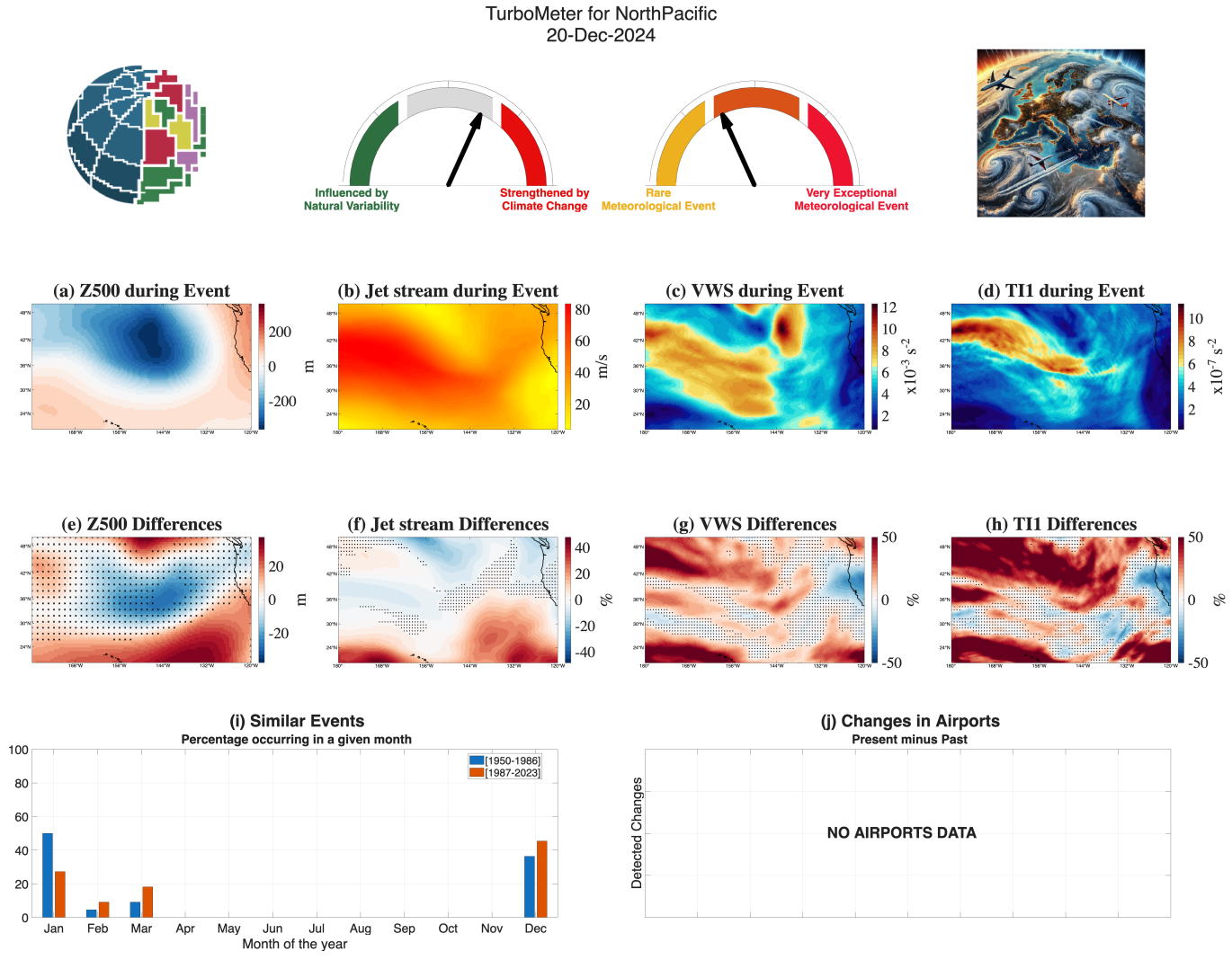


Figure 6. TurboMeter analysis for the North Pacific turbulence event on 20 December 2024. Panels (a–d) show the observed atmospheric conditions during the event, whereas panels (e–h) present the circulation-conditioned differences between the historical (1950–1986) and present-day (1987–2023) analogues. Panel (i) reports the monthly distribution of analogue occurrence for the two climate periods, while panel (j) summarizes the changes in near-surface atmospheric variables over the available airports. Black stippling denotes regions where the differences are not statistically significant at the 95% confidence level.

~~TI1 differences (Figure **??**(f)) show similar spatial patterns of the horizontal deformation (Figure **??**(h)), thus suggesting that~~ atmospheric circulation. The largest changes appear in the upper-level dynamical diagnostics. Although the jet stream exhibits only moderate strengthening (Fig. 6f), widespread and statistically significant increases ($>50\%$) in vertical wind shear are observed over large portions of the basin (Fig. 6g). These changes translate into a pronounced enhancement of TI1 (Fig. 6h,

$> 50\%$), whose spatial pattern closely follows that of the vertical wind shear anomalies, indicating that the strengthened turbulence-favourable environment is primarily associated with modifications of the ~~most important contribution to turbulence in similar episodes is related especially to TI1, vertical shear, and deformation which show widespread positive anomalies, particularly in the region where more events are reported (Figure 5). Figure ??(i) suggests no clear seasonal changes, with similar distribution of events over winter. The gauge indicators at the top of Figure ?? classify the 25 February 2024 event as likely influenced by both human-driven climate changeand natural variability and being classified as an exceptionalmeteorological event~~upper-level dynamical structure rather than substantial changes in the jet position itself.

The attribution gauge indicates that the event was strongly strengthened by climate change, whereas the rarity gauge classifies the synoptic configuration as highly exceptional. The seasonal distribution of the analogues (Fig. 6i) remains concentrated during the boreal cold season, with both historical and present-day analogues occurring predominantly during December and January. This consistency supports the circulation-conditioned nature of the attribution and indicates that the comparison is performed between analogues representative of the same seasonal circulation regime. Again, although airport-scale diagnostics (Fig. 6j) are not available for this upper-level event, the panel is retained to preserve the standard TurboMeter layout.

The ~~observed changes are also evident by separately looking at the composite fields for the past and the present periods (Figure ??~~additional surface diagnostics (Fig. 7) confirm that the analogues retain nearly identical large-scale circulation patterns, with only weak differences in the Z500 field (Fig. 7d). In ~~the past (panels a, c, e)zonal bands of enhanced TI1, VWS, and DEF are observed following the mean jet position~~ contrast, sea surface temperatures exhibit widespread positive anomalies across most of the North Pacific basin (Fig. 7h), with statistically significant warming extending over much of the subtropical and mid-latitude Pacific. Surface wind speeds also display moderate positive anomalies over the central ~~North Pacific.In contrast, composites for the present period (panels b, d, f)reveal a modified jet structure, with indications of both intensification and spatial redistribution of turbulence-favorable conditions, particularly toward the central and eastern sectors of the basin.Such patterns are consistent with increased jet variability in intensity and northward shift which have been linked in previous studies to anthropogenically forced climate change (Keel et al., 2024).~~ basin (Fig. 7l), indicating a slightly more energetic lower-tropospheric environment under present-day climate conditions. These results suggest that present-day analogues evolve over a systematically warmer ocean while preserving nearly identical synoptic circulation.

Furthermore, CAPE remains generally modest throughout the basin, with only localized statistically significant increases near the eastern boundary of the domain (Fig. 8d), in agrement with the spatial distribution of the observed turbulence reports (Fig. 5). CIN exhibits comparatively weak and spatially fragmented differences (Fig. 8h), indicating that large-scale convective instability undergoes only limited modifications between the historical and present-day analogues. By contrast, total column water vapour displays a coherent increase across much of the North Pacific (Fig. 8l), consistent with the enhanced atmospheric moisture expected under a warmer climate. These results indicate that the enhanced turbulence environment over the North Pacific is primarily associated with changes in the upper-level dynamical structure acting within a warmer and moister atmospheric background. Unlike the North Atlantic case, where the increase in atmospheric moisture is concentrated over specific sectors of the basin, the North Pacific exhibits a more spatially homogeneous thermodynamic response, whereas the dominant contribution to the enhanced turbulence signal remains the widespread increase in vertical wind shear.

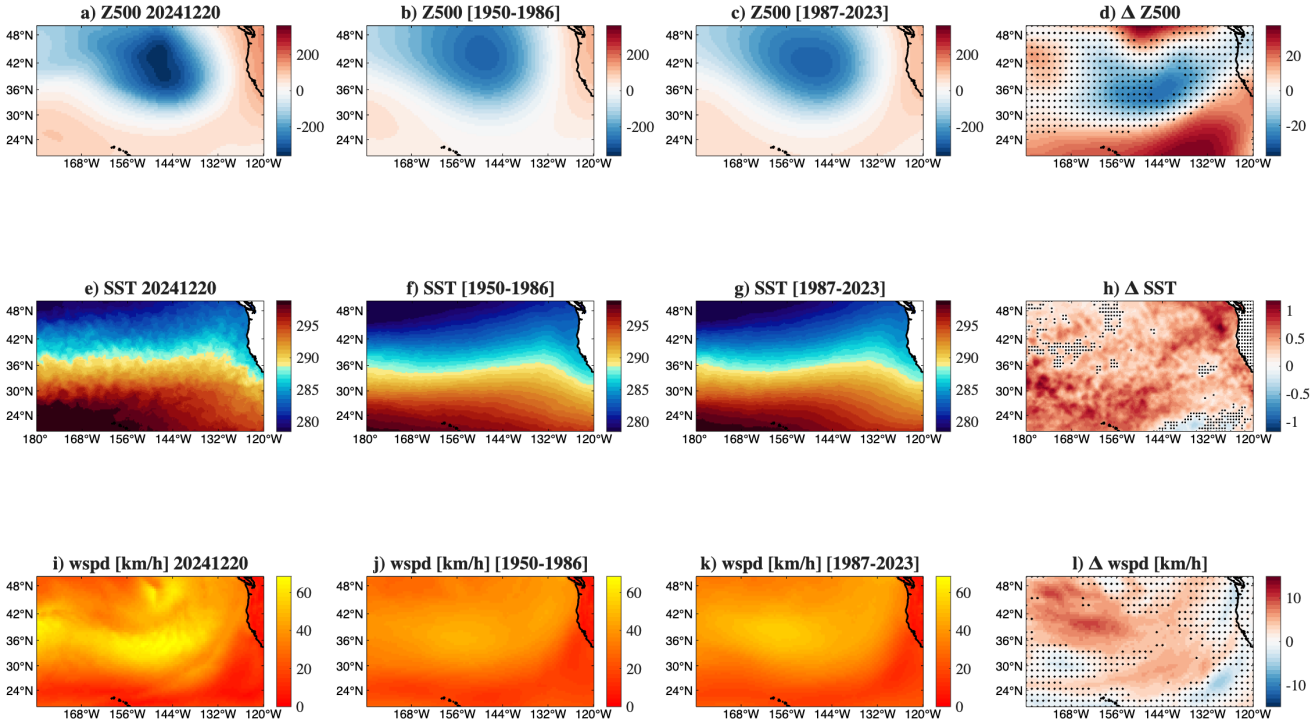


Figure 7. ~~Analogue-based results~~ Additional atmospheric and surface diagnostics for the ~~day 2024-12-20 over the~~ North Pacific ~~region~~analogues. Panels ~~show~~ (~~a~~a–d) ~~500 hPa~~ show the 500-hPa geopotential height ~~anomalies, (b~~Z500) for the ~~Ellrod index TH~~observed event, ~~(c)~~ the ~~vertical wind shear~~ historical analogue composite (~~VWS~~1950–1986), ~~and (d)~~ the ~~horizontal deformation~~ present-day analogue composite (~~DEF~~1987–2023)~~during the event~~, and the corresponding ~~climate change signals present minus past~~ present-minus-past differences. Panels (~~panels (e~~e–h) ~~,~~ show the same for Sea Surface Temperature (~~f~~SST), while panels (~~g~~i–l) ~~, and (h), respectively)~~for 10-m surface wind speed. ~~Panels (i) and (j) represent~~ Black stippling denotes regions where the ~~monthly distribution in~~ differences are not statistically significant at the ~~two periods and the changes observed in nearby airports if present~~95% confidence level.~~The dials above indicate attribution categories: influence of climate change (left) and statistical rarity (right) of the atmospheric meteorological configuration.~~

By considering all the 425 MOG turbulence reports (EDR ≥ 0.2 m$^{2/3}$ s^{-1}) in the North Pacific region occurred in 2024 (see Supplementary Materials) we observe that there are no events for which the meteorological conditions ~~have been strengthened~~ strengthened uniquely by human-driven climate change, while 19% (81 over 425) have been mostly strengthened by human-driven climate change, and the remaining 81% (344 over 425) have been likely influenced by both human-driven climate change and natural variability. We do not detect any event only driven by natural variability and for all events we have medium-to-high confidence in our claims.

~~Analogue-based results for the day 2024-12-20 over the North Pacific region. a) composite TI1 during the past period (1950–1986), b) composite TI1 during the present period (1987–2023), c) composite VWS during the past period (1950–1986), d) composite VWS during the present period (1987–2023), e) composite DEF during the past period (1950–1986), f) composite DEF during the present period (1987–2023).~~

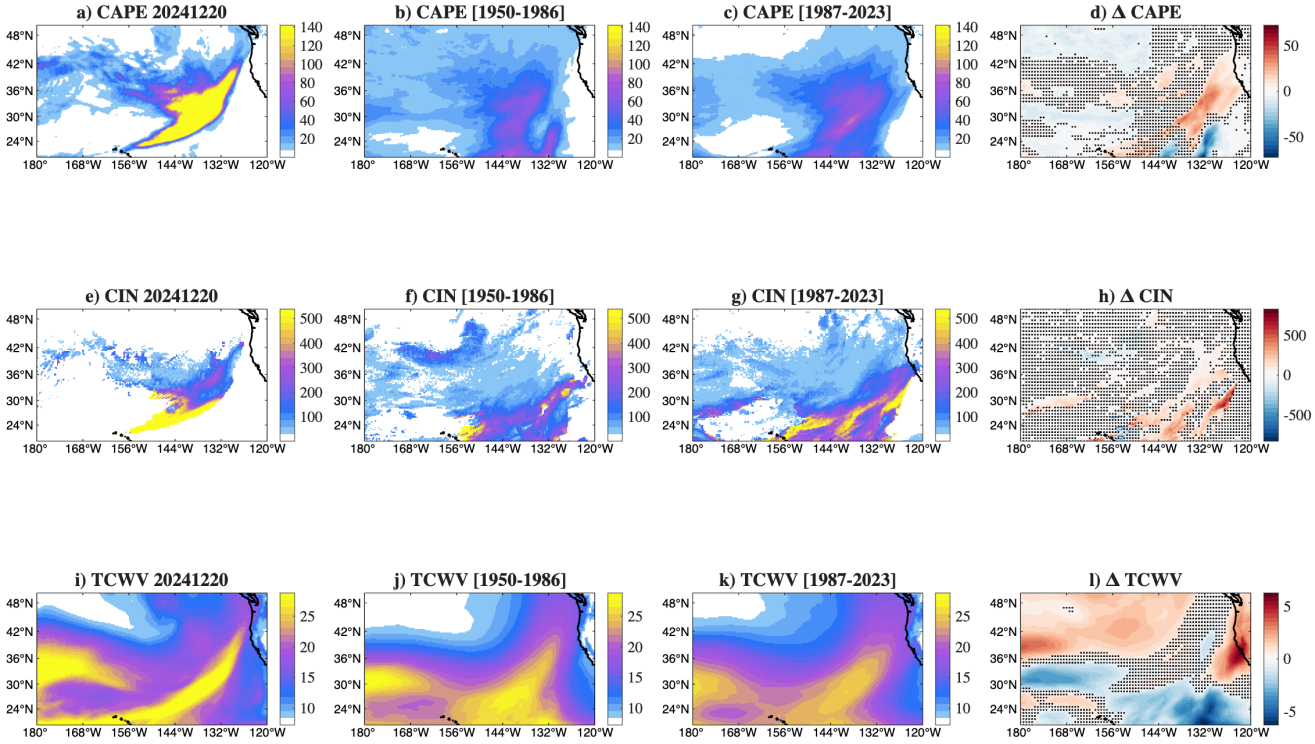


Figure 8. Additional thermodynamical diagnostics for the North Pacific analogues. Panels (a–d) show the Convective Available Potential Energy (CAPE) for the observed event, the historical analogue composite (1950–1986), the present-day analogue composite (1987–2023), and the corresponding present-minus-past differences. Panels (e–h) show the same for Convective Inhibition (CIN), while panels (i–l) for Total Column Water Vapour (TCWV). Black stippling denotes regions where the differences are not statistically significant at the 95% confidence level.

3.3 East Asia

East Asia represents one of the most dynamically complex aviation corridors, where strong upper-level jet streams interact with intense baroclinicity, subtropical moisture transport, and frequent convective activity. For the East Asia region, 150 MOG turbulence ~~events~~ reports (EDR ≥≥ 0.2 $m^{2/3}$ s^{-1}) from the NOAA MADIS archive were recorded ~~in~~ during 2024, with 12 April 2024 corresponding to the day with the highest number of ~~events~~ reports (41). As shown in ~~Figure~~Fig. 9, ~~the majority of~~

events are concentrated near the Japanese coast. most turbulence reports are concentrated along the Japanese archipelago and the adjacent western North Pacific, closely following the position of the upper-level jet.

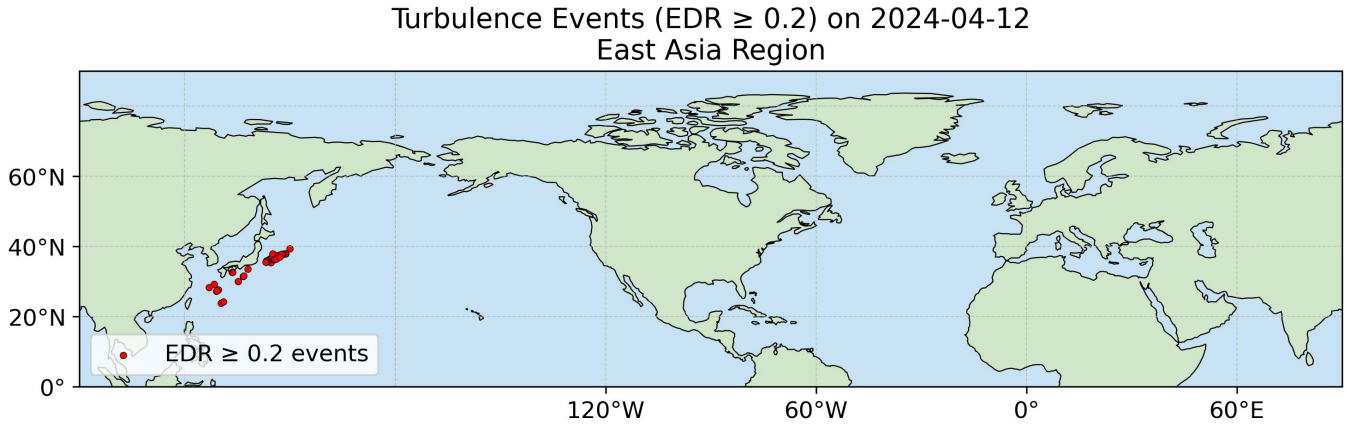


Figure 9. Distribution of the moderate-or-greater (MOG) turbulence events reports (EDR ≥≥ 0.2 $m^{2/3}$ s^{-1}) from the NOAA MADIS archive on 2024-04-12 12 April 2024 over the East Asia region.

The geopotential height anomalies (Figure **??**(a)) shows a broad-scale meridional gradient over East Asia , consistent with astrengthened circulation-conditioned attribution analysis for this event is summarized in Fig. 10. The observed atmospheric configuration is characterized by a broad upper-level westerly flow rather than a sharply defined synoptic trough. TI1 (Figure **??**(b)) reveals a narrow and elongated band of high values extending zonally across eastern China, the Korean Peninsula, and Japan, closely aligned with the average climatological position of the East Asian jet stream. Co-located maxima in ridge extending across East Asia (Fig. 10a) and a strong subtropical jet exceeding 60 m s^{-1} (Fig. 10b). Enhanced vertical wind shear and horizontal deformation (Figure **??**(develops along the equatorward flank of the jet (Fig. 10c), producing elevated TI1 values (Fig. 10d) over Japan and the adjacent western North Pacific.

The analogues reproduce remarkably similar large-scale circulation patterns, as confirmed by the relatively weak Z500 differences (d)) evidence strong jet-core dynamics, suggesting that turbulence generation in this case is primarily associated with persistent jet intensification and sharp velocity gradients, rather than transient baroclinic wave amplification. By looking at the differences, a dipole-like anomaly pattern over East Asia is observed (Figure **??**(e)), suggesting a displacement and strengthening of the Fig. 10e). The upper-level flow. TI1, vertical shear, and deformation (Figure **??**(f),(jet also retains nearly the same spatial configuration (Fig. 10f), although modest strengthening is evident over portions of the western North Pacific. Despite these comparatively small circulation changes, the present-day analogue population exhibits coherent increases in vertical wind shear (Fig. 10g), (h)) exhibit pronounced positive anomalies along the jet axis and close to its core, confirming a substantial intensification of turbulence-favorable conditions compared to past climatology. In contrast to the North Atlantic event , the anomalies are more zonally coherent and spatially confined, consistent with the quasi-stationary nature of the East Asian jet. The seasonal distribution (Figure **??**(i)) suggests a relative shift in the timing and frequency of such events toward

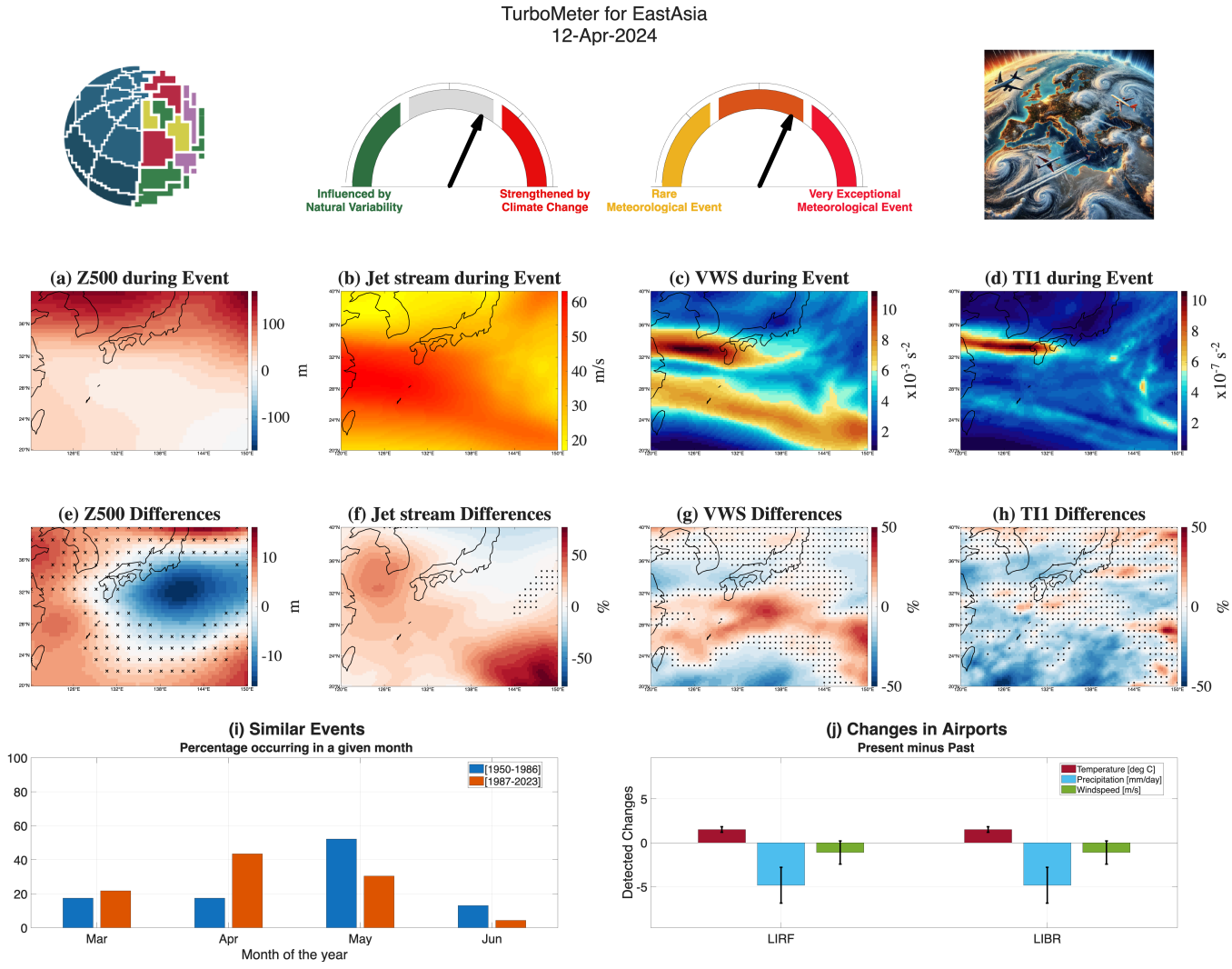


Figure 10. TurboMeter analysis for the East Asia turbulence event on 12 April 2024. Panels (a–d) show the observed atmospheric conditions during the event, whereas panels (e–h) present the circulation-conditioned differences between the historical (1950–1986) and present-day (1987–2023) analogues. Panel (i) reports the monthly distribution of analogue occurrence for the two climate periods, while panel (j) summarizes the changes in near-surface atmospheric variables over the available airports. Black stippling denotes regions where the differences are not statistically significant at the 95% confidence level.

~~early spring (April instead of May) in the present period, reflecting the seasonal maximum in East Asian jet variability. Finally, the gauge indicators (Figure **??**, top) indicate that the event is influenced by both natural variability and climate-change-related strengthening, with a tendency toward the latter, and it can be classified as a very exceptional event from a meteorological perspective. Together, these indicators frame the 12 April 2024 East Asian turbulence event as an unusually intense jet-related~~

episode, occurring in a season and region where while fragmented in TI1 (Fig. 10h). This suggest a primary role of enhanced upper-level shear, while the horizontal deformation seems to act in reducing changes in TI1.

The attribution gauge indicates that the event was strongly strengthened by climate change, while the rarity gauge classifies the circulation pattern as highly exceptional. The analogues remain confined to the spring season (Fig. 10i), although present-day analogues occur more frequently during April than during May compared with the historical climate, suggesting a modest seasonal redistribution of the circulation patterns associated with turbulence occurrence.

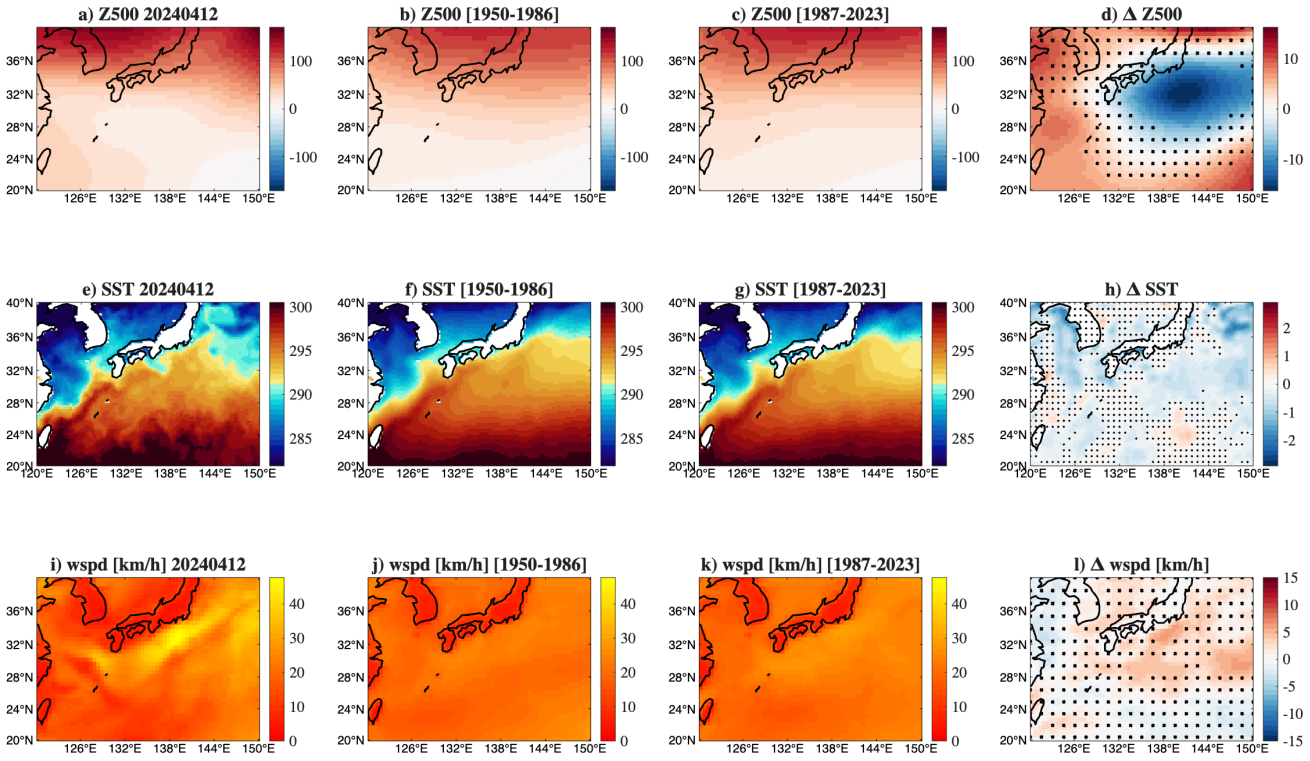


Figure 11. Additional atmospheric and surface diagnostics for the East Asia analogues. Panels (a–d) show the 500-hPa geopotential height (Z500) for the observed event, the historical analogue composite (1950–1986), the present-day analogue composite (1987–2023), and the corresponding present-minus-past differences. Panels (e–h) show the same for Sea Surface Temperature (SST), while panels (i–l) for 10-m surface wind speed. Black stippling denotes regions where the differences are not statistically significant at the 95% confidence level.

The surface diagnostics (Fig. 11) confirm that the analogues retain nearly identical large-scale circulation changes play a key dynamical role circulation patterns, while weak changes emerge in sea surface temperature and near-surface winds (Fig. 11). Unlike the North Atlantic and North Pacific cases, East Asia does not exhibit a basin-wide warming signal. Instead, SST anomalies remain comparatively weak and spatially heterogeneous, whereas moderate increases in near-surface wind speed

are observed over portions of the western North Pacific. These results suggest that surface forcing plays a less dominant role in this region than over the major oceanic flight corridors.

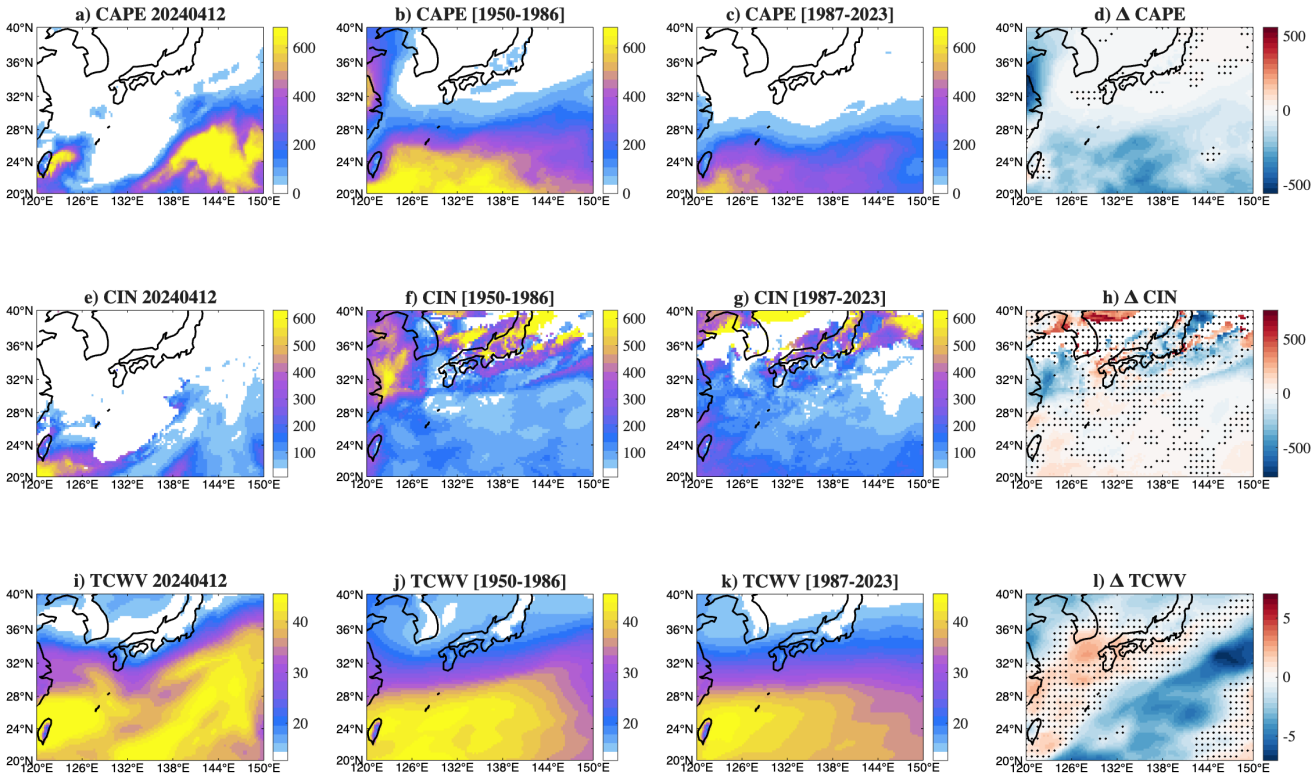


Figure 12. ~~Analogue-based results~~ Additional thermodynamical diagnostics for the ~~day 2024-04-12 over the~~ East Asia ~~region~~analogues. Panels ~~show~~ (~~a~~a–d) ~~500 hPa geopotential height anomalies,~~ show the Convective Available Potential Energy (~~b~~CAPE) for the ~~Ellrod index TH~~observed event, ~~(c)~~ the ~~vertical wind shear~~ historical analogue composite (~~VWS~~1950–1986), ~~and (d)~~ the ~~horizontal deformation~~ present-day analogue composite (~~DEF~~1987–2023)~~during the event~~, and the corresponding ~~climate change signals present minus past~~ present-minus-past differences. Panels (~~panels (e~~e–h) ~~,~~ show the same for Convective Inhibition (~~f~~CIN), while panels (~~g~~i–l) ~~, and~~ for Total Column Water Vapour (~~h~~TCWV)~~, respectively)~~. ~~Panels (i) and (j) represent~~ Black stippling denotes regions where the ~~monthly distribution in~~ differences are not statistically significant at the ~~two periods and the changes observed in nearby airports if present~~95% confidence level.~~The dials above indicate attribution categories: influence of climate change (left) and statistical rarity (right) of the atmospheric meteorological configuration.~~

~~By separately looking at the composite fields for the past and the present periods (Figure ??)we can see that in the past period (1950–1986)(panels a, c, e) the jet stream~~ The thermodynamic diagnostics reveal a more structured response than observed over the two oceanic flight corridors. CAPE exhibits localized negative changes (Fig. 12d), while CIN shows regionally

changes (Fig. 12h). Total column water vapour (Fig. 12l) also is characterized by ~~a relatively narrow and zonally elongated band with enhanced TI1, VWS, and DEF centered between approximately 32°N and 36°N, reflecting the jet structure, with turbulence-favorable conditions largely confined to the jet core. In contrast, the present-period composites (panels b, d, f) show a systematic intensification and meridional broadening of all three diagnostics. Enhanced values extend over a wider latitudinal range and are more pronounced downstream of the East Asian jet exit region, indicating increased jet variability, stronger shear zones, and more persistent deformation fields. Analogue-based results for the day 2024-04-12 over the East Asia region. a) composite TI1 during the past period (1950–1986), b) composite TI1 during the present period (1987–2023), c) composite VWS during the past period (1950–1986), d) composite VWS during the present period (1987–2023), e) composite DEF during the past period (1950–1986), f) composite DEF during the present period (1987–2023).~~ slightly increased moisture over East Asia and reduced values farther offshore. Thus, these results indicate that the strengthened turbulence-favourable environment over East Asia is associated not only with enhanced upper-level shear but also with regional and localized changes in atmospheric moisture, suggesting a stronger coupling between upper-level dynamics and regional thermodynamic processes than observed over the North Atlantic and North Pacific.

By considering all the 150 MOG turbulence reports (EDR $\geq$ 0.2 $m^{2/3}$ s^{-1}) in the East Asia region (see Supplementary Materials), we observe that there are no events for which the meteorological conditions have been strengthened uniquely by human-driven climate change, while the 73% (109 over 150) have been mostly strengthened by human-driven climate change, and the remaining 27% (41 over 150) have been likely influenced by both human-driven climate change and natural variability. We do not detect any event only driven by natural variability and for all events we have medium-to-high confidence in our claims.

3.4 Continental United States (CONUS)

The continental United States (CONUS) encompasses one of the most dynamically diverse aviation environments, where strong upper-level jets interact with complex orography, frontal systems, deep convection, and subtropical moisture transport. Consequently, turbulence observed over this corridor may arise from a broad spectrum of interacting dynamical processes, providing a particularly challenging test case for the circulation-conditioned attribution framework.

For the CONUS region, 1905 MOG turbulence ~~events~~ reports (EDR ~~$\geq$~~$\geq$ 0.2 $m^{2/3}$ s^{-1}) from the NOAA MADIS archive were recorded ~~in~~ during 2024, with 26 March 2024 corresponding to the day with the highest number of ~~events~~ reports (332). As shown in ~~Figure~~Fig. 13, ~~the majority of events~~ most turbulence reports are concentrated over the southeastern United States, particularly over Georgia and Alabama, ~~just north of Florida~~immediately north of the Gulf of Mexico, a region characterized by the interaction between subtropical moisture transport and strong upper-level dynamics.

~~The geopotential height field (Figure **??**(a)) shows a well-defined large-scale trough over the western and central CONUS, likely related with an active baroclinic wave and strong meridional flow. Downstream of the trough, an intense and curved jet streak is evident in TI1 (Figure **??**(b)), extending from northern Mexico across~~

The observed atmospheric configuration is characterized by a deep upper-level trough extending across western North America (Fig. 14a), producing a strong southwesterly jet over northern Mexico and the central United States ~~toward the eastern~~

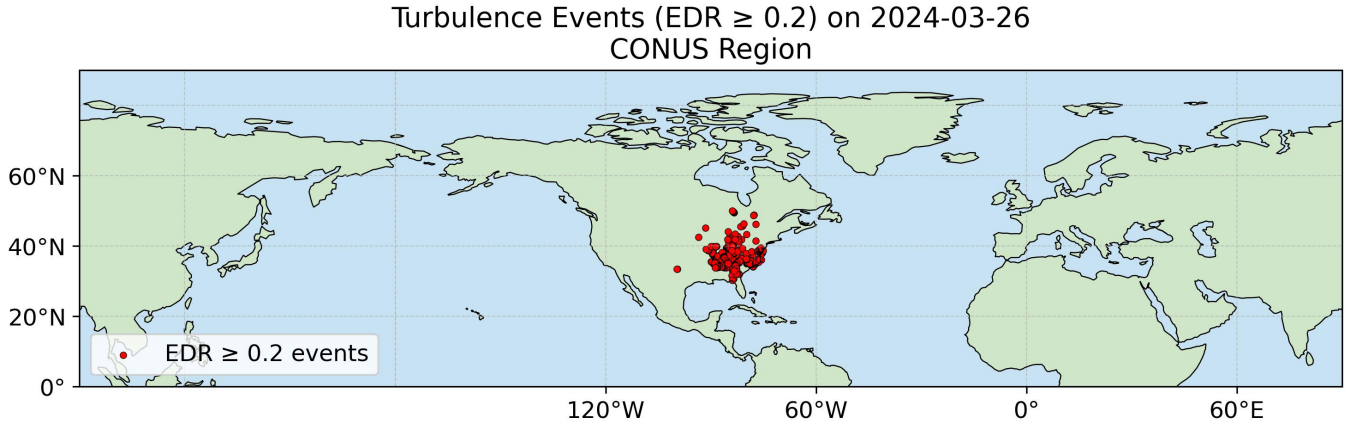


Figure 13. Distribution of ~~the~~ moderate-or-greater (MOG) turbulence ~~events~~ reports (EDR ~~≥~~≥ 0.2 $m^{2/3}$ s^{-1}) from the NOAA MADIS archive on ~~2024-03-26~~ 26 March 2024 over the CONUS region.

~~part.Maxima in~~ (Fig. 14b). The resulting upper-level shear generates an elongated band of enhanced vertical wind shear ~~and horizontal deformation (Figure ??~~((Fig. 14c), ~~(d)) are mostly co-located with this jet streak, particularly along its equator-ward flank and exit region. These features are typical of springtime synoptic systems over North America and provide a favorable environment for the generation of CAT. Geopotential height differences (Figure ??(e)) highlight an amplified wave pattern,with negative anomalies over the northward CONUS and positive anomalies downstream, consistent with enhanced trough–ridge contrast. TI1, vertical shear, and deformation (Figure ??(f)~~which closely coincides with elevated values of TI1 (Fig. 14d).

The analogues reproduce remarkably similar large-scale circulation patterns, as indicated by the relatively weak differences in Z500 (Fig. 14e),~~(g),(h)) show marked positive anomalies (up to 50%)along the jet corridor, confirming a substantial strengthening of turbulence-relevant dynamical processes compared to the past.~~ . The ~~spatial structure of these anomalies reflects the transient and highly dynamical nature of North American storm-track systems. Figure ??(~~upper-level jet also undergoes only moderate modifications (Fig. 14f)~~emphasizes a peak of occurrence in March for the past, consistent with the peak in baroclinic activity and jet variability over the CONUS during the winter–spring transition. The comparison with the present period highlights a relative increase in April occurrences, almost balancing March occurrences.Finally, based on these results the event is influenced by both natural variability and climate-change-related strengthening, with a tendency toward the latter,~~ , whereas considerably larger increases are observed in vertical wind shear (Fig. 14g). These dynamical changes translate into widespread positive TI1 anomalies (Fig. 14h), particularly over the southern United States and the Gulf of Mexico, indicating that the strengthened turbulence-favourable environment is primarily associated with enhanced upper-level shear.

The attribution gauge indicates that the event was strongly strengthened by anthropogenic climate change while the rarity gauge classifies the associated circulation pattern as highly exceptional. The analogues remain concentrated during the boreal spring (Fig. 14i), with present-day analogues occurring slightly more frequently during April than in the ~~event being not~~

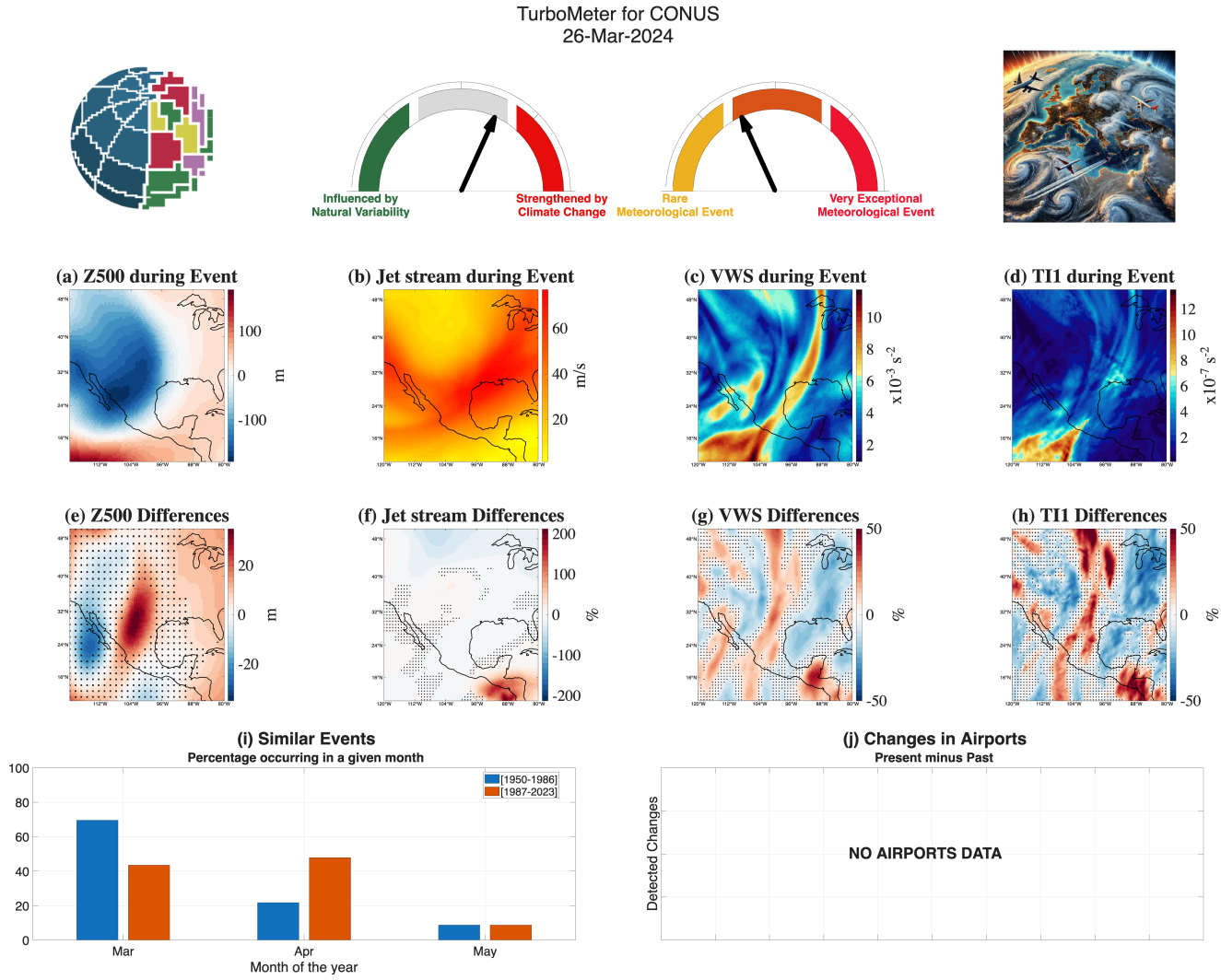


Figure 14. TurboMeter analysis for the CONUS turbulence event on 26 March 2024. Panels (a–d) show the observed atmospheric conditions during the event, whereas panels (e–h) present the circulation-conditioned differences between the historical (1950–1986) and present-day (1987–2023) analogues. Panel (i) reports the monthly distribution of analogue occurrence for the two climate periods, while panel (j) summarizes the changes in near-surface atmospheric variables over the available airports. Black stippling denotes regions where the differences are not statistically significant at the 95% confidence level.

~~very exceptional from a meteorological standpoint.~~historical period, suggesting a modest seasonal redistribution of favourable circulation patterns.

The surface diagnostics (Fig. 15) confirm that the analogues retain highly comparable synoptic-scale circulation patterns (Fig. 15d). In contrast to the predominantly oceanic flight corridors, the CONUS case exhibits coherent warming of the

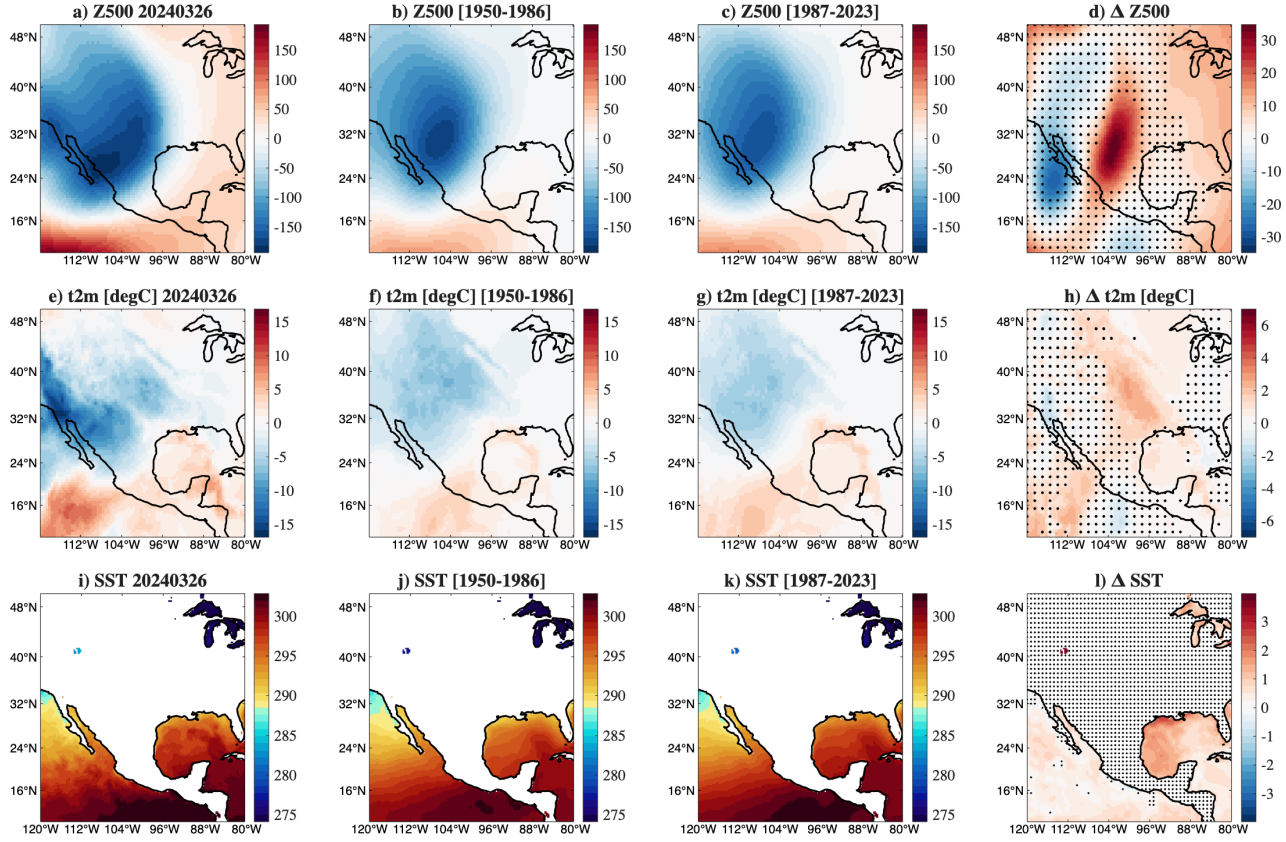


Figure 15. Additional atmospheric and surface diagnostics for the CONUS analogues. Panels (a–d) show the 500-hPa geopotential height (Z500) for the observed event, the historical analogue composite (1950–1986), the present-day analogue composite (1987–2023), and the corresponding present-minus-past differences. Panels (e–h) show the same for Sea Surface Temperature (SST), while panels (i–l) for 10-m surface wind speed. Black stippling denotes regions where the differences are not statistically significant at the 95% confidence level.

near-surface atmosphere over large portions of the southern United States (Fig. 15h), accompanied by positive sea surface temperature anomalies over the Gulf of Mexico (Fig. 15l). Together, these ~~indicators frame the 26 March 2024 CONUS event as an unusually intense springtime jet~~changes indicate that the circulation analogues evolve within a warmer land–~~trough interaction, embedded within a dynamically active and increasingly amplified midlatitude circulation regime~~ocean environment under present-day climate conditions.

~~In detail, we observe that the composite fields for the past period (Figure ??, panels a, c, e)depict a climatological jet characterized by a relatively coherent and zonally oriented band of enhanced TI1, VWS, and DEF across the northern and central United States . Turbulence-favorable conditions are largely confined to the mean jet position, reflecting a large-scale flow configuration. In contrast,~~ The thermodynamical diagnostics reveal the strongest thermodynamic response among the four analysed flight corridors (Fig. 16). CAPE exhibits pronounced positive anomalies over the Gulf of Mexico and the

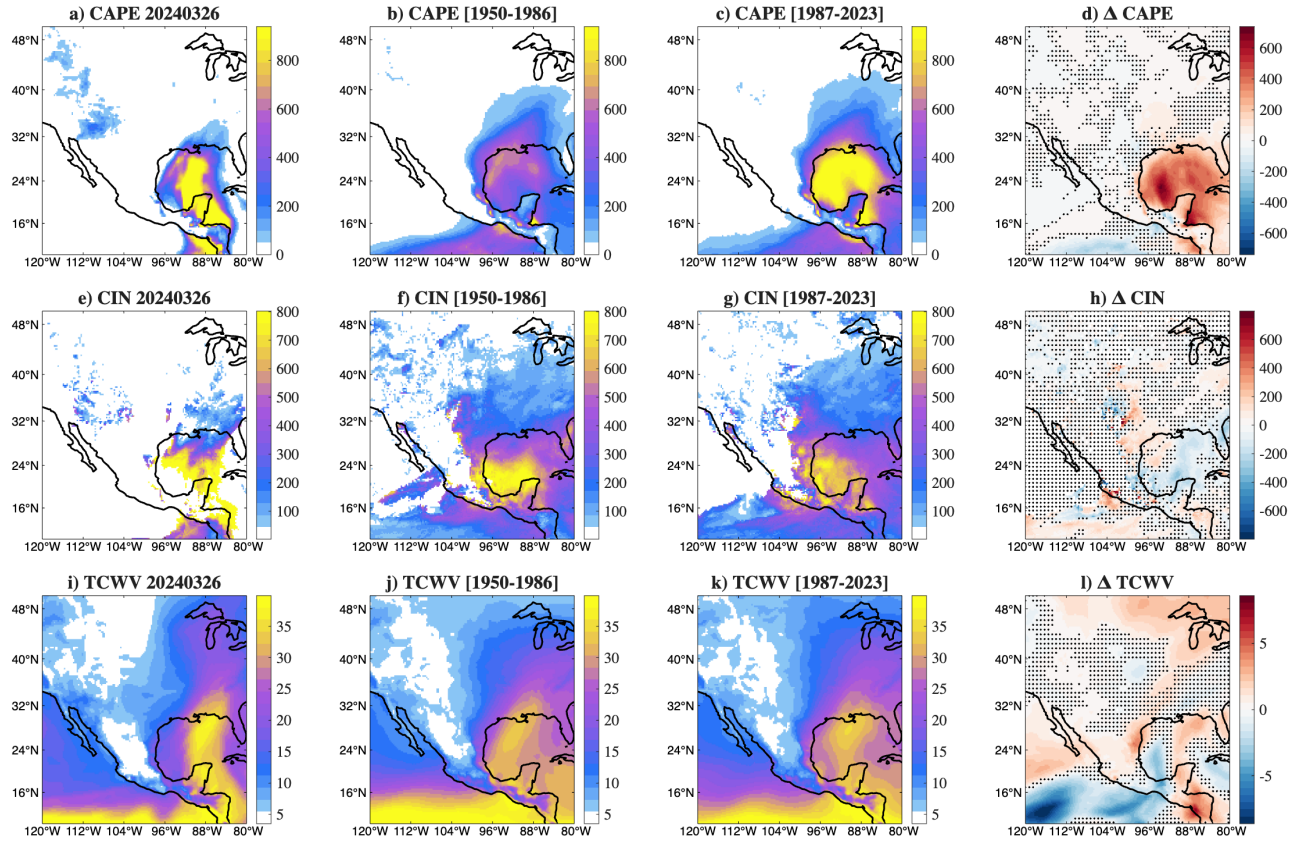


Figure 16. ~~Analogue-based results~~ Additional thermodynamical diagnostics for the ~~day 2024-03-26 over the~~ CONUS ~~region~~analogues. Panels ~~show~~ (~~a~~a–d) ~~500 hPa geopotential height anomalies,~~ show the Convective Available Potential Energy (~~b~~CAPE) for the ~~Ellrod index TH~~observed event, ~~(c)~~ the ~~vertical wind shear~~ historical analogue composite (~~VWS~~1950–1986), ~~and (d)~~ the ~~horizontal deformation~~ present-day analogue composite (~~DEF~~1987–2023)~~during the event~~, and the corresponding ~~climate change signals present minus past~~ present-minus-past differences. Panels (~~panels (e~~e–h) ~~,~~ show the same for Convective Inhibition (~~f~~CIN), while panels (~~g~~i–l) ~~, and~~ for Total Column Water Vapour (~~h~~TCWV)~~, respectively)~~. ~~Panels (i) and (j) represent~~ Black stippling denotes regions where the ~~monthly distribution in~~ differences are not statistically significant at the ~~two periods and the changes observed in nearby airports if present~~95% confidence level.~~The dials above indicate attribution categories: influence of climate change (left) and statistical rarity (right) of the atmospheric meteorological configuration.~~

~~present-period composites (Figure ??, panels b, d, f)reveal a clear intensification and spatial reorganization of all three diagnostics.Enhanced TH, VWS, and DEF extend over a broader longitudinal and latitudinal range, particularly across the central and eastern CONUS, indicating increased jet variability, stronger local shear zones, yet, the absolute maximum of VWS has decreased, and more persistent deformation fields in the upper troposphere~~southeastern United States (Fig. 16d), indicating increasingly favourable conditions for convection. Consistently, CIN displays localized reductions over portions of the same region (Fig. 16h),

suggesting a weaker inhibition of convective development. Total column water vapour also increases over much of the southern United States and the Gulf of Mexico (Fig. 16l), indicating enhanced atmospheric moisture availability under present-day climate conditions. These indicate that the circulation-conditioned strengthening of the turbulence-favourable environment over CONUS results from the combined influence of enhanced upper-level dynamics and a warmer, moister, and locally more unstable lower atmosphere. Compared with the North Atlantic and North Pacific cases, where the dominant signal is primarily associated with upper-level dynamics, the CONUS event exhibits a substantially stronger coupling between atmospheric dynamics and regional thermodynamic conditions while the large-scale circulation remains remarkably consistent between the historical and present-day analogues.

~~Analogue-based results for the day 2024-03-26 over the CONUS region. a) composite TI1 during the past period (1950–1986), b) composite TI1 during the present period (1987–2023), c) composite VWS during the past period (1950–1986), d) composite VWS during the present period (1987–2023), e) composite DEF during the past period (1950–1986), f) composite DEF during the present period (1987–2023).~~

By considering all the 1905 MOG turbulence reports (EDR ≥ 0.2 $m^{2/3}$ s^{-1}) in the CONUS region that occurred in 2024 (see Supplementary Materials), we observe that more than 27% (522 over 1905) of events have been strengthened by human-driven climate change, 48% (922 over 1905) have been mostly strengthened by human-driven climate change, and the remaining 25% (461 over 1905) have been likely influenced by both human-driven climate change and natural variability. We do not detect any event only driven by natural variability and for all events we have medium-to-high confidence in our claims.

4 Discussion

~~This study applies an~~ An analogue-based ~~diagnostic framework~~ attribution framework is presented to investigate the dynamical drivers, spatial characteristics, and climatic context of moderate-or-greater (MOG) turbulence events across four major aviation regions: the North Atlantic, North Pacific, East Asia, and the Continental United States (CONUS). ~~We need to acknowledge that there is a regional imbalance in the reported events, as the NOAA MADIS dataset is dominated by reports from U.S. airlines. Consequently, more than 50% of the turbulence events occur over the continental United States (CONUS), while substantially fewer cases are available over other regions, particularly East Asia, which is represented by only about 150 events. This imbalance may affect the interpretation of the observed regional contrasts, thus the results calculated for CONUS are more representative, and therefore more robust than the results for other regions. For East Asia specifically, the analysis is based on data from only four days (February, April, May, and July), with no wintertime cases included, despite the fact that clear-air turbulence is typically more frequent during winter. These limitations primarily reflect current data availability; however, future work would benefit from improved spatial and seasonal sampling, especially over East Asia and other data-sparse regions. Nevertheless, several coherent signals emerge that are relevant for both turbulence prediction and climate-change attribution.~~

~~Across all regions, days with the highest number of reported MOG turbulence events are consistently~~ Several physically coherent signals consistently emerge across all four flight corridors. Days with the largest number of MOG turbulence reports are associated with enhanced upper-tropospheric jet activity, ~~as diagnosed by high values of the Ellrod index (TI1),~~ vertical

wind shear, and ~~horizontal deformation. These diagnostics highlight the central role of jet streaks, entrance and exit regions, and sharp horizontal velocity gradients in controlling the spatial distribution and intensity of CAT at cruise altitudes.~~ increased Ellrod index values. The close spatial correspondence between ~~turbulence diagnostics and~~ the observed EDR reports ~~provides independent~~ and the diagnosed turbulence fields provides further support for the physical relevance of the ~~selected metrics.~~

~~The North Atlantic and North Pacific case studies are characterized by turbulence generation within highly transient, baroclinic storm-track environments. Over the~~ adopted diagnostics. The additional surface and thermodynamic analyses further indicate that these dynamical changes generally develop within warmer and moister atmospheric environments, although the associated thermodynamic response varies substantially among regions. Independent satellite brightness temperatures (not shown) further suggest that the dominant cloud environments differ among regions, with CONUS events more frequently associated with cold cloud tops, whereas North Atlantic and North ~~Atlantic, turbulence is tightly linked to an amplified trough–ridge system and a strengthened jet aligned with the main transoceanic flight corridor. Over the North Pacific , turbulence occurs within a deep cyclonic anomaly associated with winter storm-track activity, with strong deformation and vertical shear extending over a broad area. In both regions, present-minus-past differences reveal deeper geopotential height anomalies and widespread increases in turbulence-relevant diagnostics, indicating an intensification of synoptic-scale dynamics rather than a simple spatial displacement.~~ Pacific events are more often associated with warm brightness temperatures, consistent with a larger proportion of clear-air events.

~~In contrast, the East Asia case highlights a different physical mechanism for the considered day, dominated by quasi-stationary jet intensification rather than transient baroclinic waves. Turbulence enhancements are spatially confined along the climatological jet axis and exhibit strong zonal coherence. The associated climate-change signal primarily reflects a strengthening and meridional displacement of the East Asian jet,~~ The two oceanic flight corridors, namely the North Atlantic and North Pacific, exhibit remarkably consistent behaviour. In both cases, the analogues preserve nearly identical synoptic-scale circulation patterns while developing over systematically warmer ocean surfaces, favoring moisture and vertical shears. The increased sea surface temperatures are accompanied by coherent increases in total column water vapour, whereas changes in CAPE and CIN remain comparatively weak and spatially fragmented. These results suggest that the primary climate signal over the oceanic corridors is not associated with substantial changes in large-scale convective instability, but rather with a warmer and moister atmospheric background that accompanies enhanced upper-level wind shear and increased turbulence diagnostics. Interestingly, the strengthening of TI1 is much more closely associated with enhanced vertical wind shear than with substantial modifications of the jet-stream position itself, indicating that climate change primarily alters the dynamical structure of the upper-tropospheric flow while preserving the overall synoptic organization.

East Asia exhibits a somewhat different behaviour. While the circulation-conditioned attribution still indicates that enhanced vertical wind shear remains the dominant dynamical driver of the strengthened turbulence environment, the thermodynamic response is different than over the oceanic basins. Localized increases in CAPE, regional changes in CIN, and a coherent redistribution of atmospheric moisture suggest that modifications of the thermodynamic environment accompany the strengthening of the upper-level dynamics. Although TurboMeter does not distinguish among individual turbulence-generation mechanisms, these results are broadly consistent with the ~~sensitivity of this circulation system to changes in meridional temperature gradients~~

during the spring transition seasoncomplex multiscale interactions between jet dynamics, subtropical moisture transport, and convective activity that characterize the East Asian upper troposphere (Kim and Chun, 2012; Kim et al., 2014; Trier et al., 2020; Kim et al.,
590 .

The considered day for CONUS further emphasizes the role of seasonal storm-track dynamics , with turbulence associated with an amplified springtime trough–jet interaction. Compared to the oceanic regions, this meteorological condition is less exceptional in terms of CONUS case represents the strongest coupling between atmospheric dynamics and thermodynamics. Compared with the oceanic corridors, the analogues develop within a markedly warmer lower atmosphere, accompanied by
595 increased atmospheric moisture, enhanced CAPE, and locally reduced CIN over the Gulf of Mexico and the southeastern United States. These thermodynamic changes occur together with widespread increases in vertical wind shear and TI1 while the large-scale circulation rarity, yet it exhibits strong positive anomalies in TI1, vertical shear, and deformation. This finding indicates thatimpactful turbulence can arise from relatively common synoptic configurations whose intensity has increased relative to past climatologycirculation remains highly comparable between the historical and present-day analogues. The results therefore
600 suggest that, over continental regions where moisture availability and convection play a larger role, climate change modifies not only the upper-level dynamical environment but also the thermodynamic conditions within which turbulence develops.

Monthly occurrences across regions reveal that changes in turbulence occurrence are not uniform throughout the season. Oceanic regions maintain a strong winter dominance, while analogues occurrences across the four regions further indicate that climate-related changes are not limited to turbulence intensity. Oceanic corridors maintain a pronounced winter maximum,
605 whereas East Asia and CONUS exhibit maxima during transitional peaks during the transition seasons. In several cases, the more recent period shows shifts toward earlier months in the season present-day analogues show a tendency toward earlier seasonal occurrence or more concentrated seasonal peaks, suggesting that climate-driven circulation changes may be affecting not only turbulence intensity but also its seasonal timing. To our knowledge, this seasonal shift has received comparatively little attention in previous turbulence–climate attribution studies, which have primarily focused on changes in mean intensity
610 or frequency. Although further work is needed to assess this signal across datasetsand diagnostics, this seasonal shift suggests a potentially modification of the seasonal phase of the upper-tropospheric dynamical environment, implying that the timing of peak turbulencerisk may no longer align with the historical climatology. Such a shift monthly analogues distributions compared with the historical period. Although this signal requires confirmation using larger datasets, it suggests that climate change may also influence the seasonal timing of atmospheric environments favourable to aviation turbulence. Such seasonal shifts could
615 have practical implications for flight operations, including seasonal route planning, crew training emphasis, and turbulence risk management, particularly in heavily trafficked corridorsturbulence forecasting, and risk management.

Finally, the attribution gauges synthesize provide a concise synthesis of both the dynamical and statistical aspects characteristics of each event. While not all events are every analysed event is classified as meteorologically exceptional, most display a detectable contribution from climate-change-related strengthening of the large-scale flowmeasurable contribution from climate
620 change. This distinction is important, as particularly important because it indicates that increased turbulence risk may arise from stronger manifestations of commonly occurring circulation patterns, rather than from does not necessarily arise from the emergence of entirely new atmospheric statescirculation patterns. Instead, the results consistently suggest that comparable

synoptic configurations now evolve within atmospheric environments characterized by enhanced upper-level shear, increased atmospheric moisture, and, in some regions, more favourable conditions for convection.

5 Conclusions

This work demonstrates the value of an analogue-based and physically grounded framework for diagnosing ~~MOG~~ moderate-or-greater (MOG) turbulence events and assessing their relationship to climate variability and anthropogenic climate change. By integrating turbulence diagnostics, large-scale circulation patterns, and historical atmospheric analogues, the TurboMeter ~~approach provides a comprehensive~~ framework provides a physically interpretable link between observed aviation ~~impacts and their underlying dynamical causes~~turbulence and the atmospheric environments in which it develops.

Our analysis reveals that turbulence events with a detectable contribution from ~~anthropogenic~~ climate change are present across several major ~~regions~~aviation corridors, including CONUS, the North Atlantic, and East Asia (Table 1 and ~~Figure 17(a)~~Fig. 17a). In contrast, the signal is ~~less pronounced~~ comparatively weaker over the North Pacific, although regional comparisons should be interpreted with caution given the limited number of events available in some regions, particularly East Asia. ~~A substantial fraction of the analyzed days over East Asia, CONUS, and the North Atlantic (Figure 17(b)) falls into categories where turbulence is strengthened or mostly strengthened by human-induced climate change, accounting for~~ Overall, approximately 68% of the ~~events. This predominance of climate change increased turbulence has important implications for aviation safety and operations. Enhanced upper-tropospheric wind shear and jet variability increase the likelihood of CAT encounters, which remain difficult to detect and avoid. A systematic shift toward more frequent and/or more intense turbulence may therefore increase in-flight injury risk and require more frequent altitude adjustments or route deviations. From an operational perspective, such changes can increase fuel burn, flight time variability, and air traffic management complexity, highlighting the need to consider climate-driven turbulence trends in both forecasting development and long-term aviation planning A smaller but non-negligible share (about 32%) is associated with a combination of climate change and natural variability.In contrast, over the North Pacific, the majority of events (81%) are associated with~~ analysed events are classified as strengthened or mostly strengthened by anthropogenic climate change (Fig. 17b), whereas the remaining events are likely influenced by a combination of climate change and natural variability. ~~This highlights~~ These results indicate that, although natural variability continues to play an important role in shaping atmospheric circulation, anthropogenic forcing ~~increasingly modulates the occurrence and characteristics of aviation-relevant turbulence.~~ is increasingly modifying the atmospheric environments associated with aviation turbulence.

~~Our findings are consistent with Foudad et al. (2024), who used a large initial-condition ensemble of a climate model to show that observed positive trends in clear-air turbulenceover recent decades across multiple Northern Hemisphere regions are attributable to anthropogenic climate change, while internal climate variability plays an important role in other regions. Although the methods differ—the present study employs an analogue-based attribution framework rather than large ensemble simulations—the convergence of results highlights a consistent picture of the interplay between forced climate change and natural variability across regions, reinforcing the robustness of the physical interpretation. The agreement in both spatial~~

~~patterns and qualitative seasonal behavior suggests that the detected signal is not an artifact of a particular attribution framework, but rather a dynamically coherent response to large-scale circulation changes under anthropogenic forcing. Importantly, the analogue method isolates circulation-conditioned thermodynamic contributions in a way that complements large-ensemble approaches, offering an independent line of evidence for attribution.~~

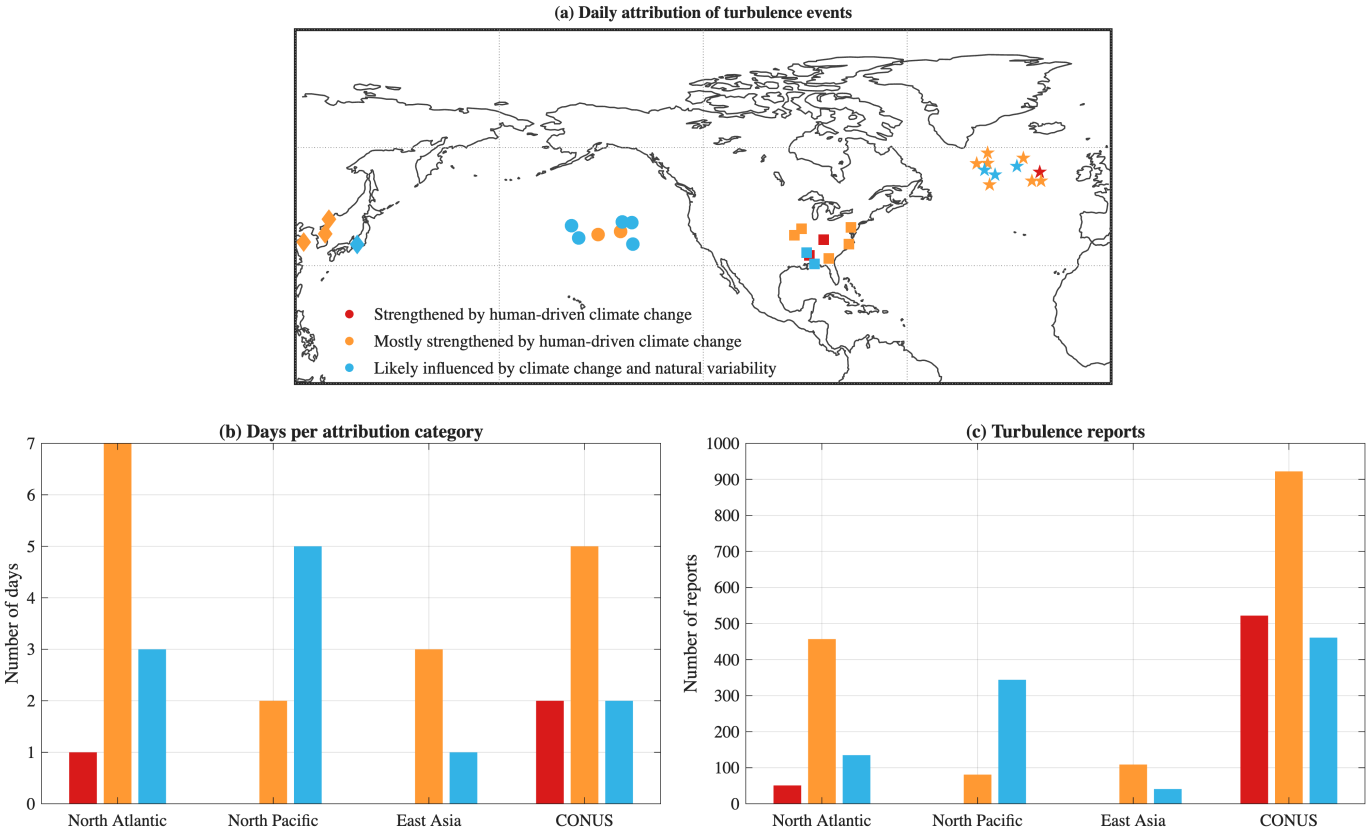


Figure 17. Summary of turbulence events and their climate attribution. (a) ~~Global~~ Geographic distribution of the analysed turbulence events, with symbols indicating event locations and ~~colors~~ colours denoting attribution categories: strengthened by anthropogenic climate change (red), mostly strengthened by anthropogenic climate change (orange), and likely influenced by both climate change and natural variability (blue). (b) Number of analysed days associated with each attribution category ~~for~~ across the ~~main regions considered (North Atlantic, North Pacific, East Asia and CONUS)~~four flight corridors. (c) Number of ~~reported~~ turbulence ~~occurrences per~~ reports (EDR≥0.2) associated with each attribution category and region.

~~The main conclusions of this study indicate that jet-stream dynamics are~~ Our findings are broadly consistent with Foudad et al. (2024), who used large initial-condition ensembles to demonstrate that the observed increase in clear-air turbulence over recent decades can largely be attributed to climate change, while natural variability remains important in several regions. Although the methodologies differ, the convergence of the results supports a physically coherent interpretation of the climate signal affecting upper-tropospheric turbulence. The analogue-based framework adopted here provides an independent observational

Region	Attribution result	# of days		# of reports (EDR≥0.2)	
		Days	Total	Reports	Total
North Atlantic	strengthened by human-driven climate change	1		51	
	mostly strengthened by human-driven climate change	7	11	457	643
	likely influenced by climate change and natural variability	3		135	
North Pacific	strengthened by human-driven climate change	0		0	
	mostly strengthened by human-driven climate change	2	7	81	425
	likely influenced by climate change and natural variability	5		344	
East Asia	strengthened by human-driven climate change	0		0	
	mostly strengthened by human-driven climate change	3	4	109	150
	likely influenced by climate change and natural variability	1		41	
CONUS	strengthened by human-driven climate change	2		522	
	mostly strengthened by human-driven climate change	5	9	922	1905
	likely influenced by climate change and natural variability	2		461	

Table 1. Summary of attribution results across all analyzed regions. For each region, the table reports the number of days classified in each attribution category and the corresponding number of turbulence reports with EDR≥0.2. No events were classified as mostly driven by natural variability or as low confidence.

perspective that complements large-ensemble climate simulations by explicitly conditioning the attribution on comparable synoptic-scale circulation patterns.

A key aspect of the TurboMeter approach is that the analogue-selection procedure relies exclusively on the large-scale atmospheric circulation represented by the 500-hPa geopotential height field. This choice intentionally constrains the synoptic environment associated with each turbulence encounter. The additional diagnostics, including sea surface temperature, near-surface temperature, upper-level wind speed, total column water vapour, CAPE, and CIN, provide a physically consistent interpretation of the selected analogues. This separation between circulation conditioning and atmospheric interpretation represents one of the principal strengths of the TurboMeter framework and allows additional diagnostics to be incorporated without modifying the usual underlying attribution methodology based on ciruclation-analogues (e.g., Faranda et al., 2024).

Across all analysed regions, the results consistently indicate that climate change primarily modifies the atmospheric environments in which aviation turbulence develops rather than the ~~dominant driver of MOG turbulence across all considered regions, with turbulence consistently linked to enhanced vertical wind shear and horizontal deformation within jet streak regions. Anthropogenic climate change appears to enhance conditions favorable to turbulence , rather than generating entirely new circulation regimes. As a result, present-day events are more likely to develop within deeper troughs, stronger jets, or more persistent jet structures than their historical analogues. The monthly occurrence of severe turbulence events is also evolving in a region-dependent manner, showing shifts in timing and frequency, particularly during transitional seasons (e.g., from winter to spring). Finally, strong turbulenceevents do not necessarily require rare atmospheric configurations, but can arise from~~

~~intensified versions of common circulation patterns.~~ large-scale circulation patterns themselves. Oceanic flight corridors are characterized by coherent increases in sea surface temperature, atmospheric moisture, and upper-level wind shear, whereas continental regions additionally exhibit stronger thermodynamic responses, including enhanced CAPE and reduced CIN. Although the relative importance of these processes varies among regions, the strengthening of upper-level vertical wind shear emerges as the most robust dynamical signature associated with enhanced turbulence-favourable environments.

~~The proposed turbulence attribution framework can be further extended and strengthened in several ways. In this study,~~ We need to underline some limitations of the present framework. Aviation turbulence encompasses multiple physical mechanisms, including clear-air turbulence, mountain-wave turbulence, convectively induced turbulence, near-cloud turbulence, and gravity-wave breaking, which frequently coexist and interact. While the analogue framework successfully constrains the large-scale atmospheric circulation associated with observed turbulence events, ERA5 cannot explicitly resolve many of the mesoscale and microscale processes responsible for individual aircraft-scale turbulence encounters. Consequently, TurboMeter should not be interpreted as attributing individual turbulence-generation mechanisms or to capture the turbulence generated by unresolved processes, such as mountain waves, partly convection, etc. Rather, it quantifies how the atmospheric environments favourable to aviation turbulence evolve under comparable synoptic circulation conditions. Furthermore, here we focus on a single clear-air turbulence diagnostic (TI1), while future work could incorporate multiple turbulence indices to better capture the diversity of physical mechanisms associated with ~~CAT~~aviation turbulence. More broadly, the framework could be extended to other turbulence types, including convectively induced turbulence, mountain-wave turbulence, and mid- and lower-tropospheric turbulence, allowing a more comprehensive assessment of turbulence risk across ~~flight phases and atmospheric regimes.~~ different flight phases (including landing and take-off). We also need to acknowledge that the analysed turbulence reports are regionally unbalanced because the NOAA MADIS dataset is dominated by observations from U.S. airlines. Consequently, more than 50% of the reported events occur over CONUS, whereas substantially fewer cases are available over the North Pacific and especially East Asia, which is represented by only about 150 reports. This imbalance inevitably affects the robustness of regional comparisons, making the CONUS statistics more representative than those obtained over East Asia. Furthermore, the East Asian analysis is based on only four representative days (occurring in February, April, May and July), with no wintertime cases despite the well-known winter maximum of upper-level turbulence in this region. These limitations primarily reflect the current observational availability and motivate future studies based on more spatially and seasonally homogeneous datasets.

~~Overall, these findings support the emerging evidence that~~ Nevertheless, the results presented here support the growing evidence that anthropogenic climate change is already modifying the ~~dynamical environments conducive to clear air turbulence, with important implications for flight safety, operational planning, and resilience of the global aviation system in the coming decades. By quantifying these changes, the turbulence gauges introduced in this work offer a concrete tool for investigating heightened risk periods, informing flight routing strategies, crew training, and fleet management. Furthermore, they provide a robust evidence base that can support discussions at ICAO and other aviation policy forums, helping to integrate climate-driven turbulence trends into operational guidelines and~~ atmospheric environments associated with aviation turbulence. By combining circulation-conditioned attribution with additional physical diagnostics, TurboMeter provides a flexible attribution framework that complements process-based numerical studies and offers new opportunities for turbulence characterization, risk assessment,

and long-term ~~resilience planning for the global air transport system~~climate adaptation strategies for the aviation sector. Future developments may combine the circulation-conditioned approach of TurboMeter with objective turbulence classification algorithms, higher-resolution numerical simulations, satellite observations, airborne measurements, and machine-learning approaches. Such developments would allow the relative contribution of different turbulence-generation mechanisms to be investigated while preserving the physically interpretable analogue-based framework introduced here.

Code availability

All codes used for the analysis and generating the figures can be obtained from the authors upon request.

Data availability

The data that support the findings of this study are openly available. ERA5 is the latest climate reanalysis being produced by ECMWF as part of implementing the EU- funded Copernicus Climate Change Service (C3S), providing hourly data on atmospheric, land-surface and sea-state parameters together with estimates of uncertainty from 1950 to present day. ERA5 data are available on the C3S Climate Data Store on regular latitude-longitude grids at 0.25° x 0.25° resolution at https://cds.climate.copernicus.eu/#!/home. The tele-connection indices (ENSO, AMO, NAO) are computed from the NOAA/ERSSTv5 data and retrieved from KNMI's climate explorer at https://climexp.knmi.nl/start.cgi. ACARS EDR turbulence reports were obtained from the public NOAA MADIS archive and are available at https://madis.ncep.noaa.gov. The turbulence event dataset analysed in this study was derived from these reports and is available from the authors upon reasonable request.

Author contribution

TA conceived the study, performed the analyses, and wrote the draft of the manuscript. DF conceived the study and the methodology. MF provided the suitable list of turbulence events to be analyzed. All authors contributed to discuss the results and to write the paper.

Competing interests

The authors declare that they have no conflict of interest.

Acknowledgements

TA and DF acknowledge useful discussions within the FutureMed COST Action (CA22162) community. TA received funding from Ministero dell'Università e della Ricerca under the call Fondo Italiano per la Scienza 2022-2023 (FIS-2) for the project "Mediterranean Extreme Events and Tipping elements in a changing climate on multiple spatiotemporal scales", grant number

FIS-2023-00159, CUP: D53C24005450001. DF acknowledge the European Union Horizon 2020 research and innovation programme under grant agreement no. 101003469 (XAIDA). The turbulence observations used in this study were made available to the National Oceanic and Atmospheric Administration (NOAA) through contributions from several commercial airlines, including American, Delta, Federal Express, Northwest, United, and United Parcel Service. MF thanks Thorsten Kaluza for helpful discussions and his assistance with the ACARS turbulence reports. MF and PDW acknowledge funding from the Leverhulme Trust, under Grant RPG-2023-138. MACT acknowledges the Portuguese Fundacao para a Ciencia e Tecnologia (FCT) for its financial support via the LAETA Associated Laboratory (project https://doi.org/10.54499/UID/50022/2025).

References

Alberti, T., Faranda, D., Rapella, L., Coppola, E., Lepreti, F., Dubrulle, B., and Carbone, V.: Impacts of changing atmospheric circulation patterns on aviation turbulence over Europe, Geophysical Research Letters, 51, e2024GL111 618, 2024.

Baek, S.-H., Kim, J.-H., Kim, S.-H., Lee, Y., Noh, Y.-J., and Lee, S.-M.: Characteristics of Convectively Induced Turbulence in East Asia Using Geostationary Korea Multi-Purpose Satellite-2A (GK-2A) and In Situ Aircraft Data, Journal of Geophysical Research: Atmospheres, 129, e2024JD041 671, https://doi.org/10.1029/2024JD041671, 2024.

Burbidge, R., Paling, C., and Dunk, R. M.: A systematic review of adaption to climate change impacts in the aviation sector, Transport Reviews, 44, 8–33, 2024.

Dutton, J. A.: Clear-air turbulence, aviation, and atmospheric science, Reviews of Geophysics, 9, 613–657, 1971.

Ellrod, G. P. and Knapp, D. I.: An Objective Clear-Air Turbulence Forecasting Technique: Verification and Operational Use, Weather and Forecasting, 7, 150–165, https://doi.org/10.1175/1520-0434(1992)007<0150:AOCATF>2.0.CO;2, 1992.

Ellrod, G. P. and Knox, J. A.: Improvements to an Operational Clear-Air Turbulence Diagnostic Index by Addition of a Divergence Trend Term, Weather and Forecasting, 25, 789–798, https://doi.org/10.1175/2009WAF2222290.1, 2010.

Faranda, D., Messori, G., Jezequel, A., Vrac, M., and Yiou, P.: Atmospheric circulation compounds anthropogenic warming and impacts of climate extremes in Europe, Proceedings of the National Academy of Science, 120, e2214525120, https://doi.org/10.1073/pnas.2214525120, 2023.

Faranda, D., Messori, G., Coppola, E., Alberti, T., Vrac, M., Pons, F., Yiou, P., Saint Lu, M., Hisi, A. N. S., Brockmann, P., Dafis, S., Mengaldo, G., and Vautard, R.: ClimaMeter: contextualizing extreme weather in a changing climate, Weather and Climate Dynamics, 5, 959–983, https://doi.org/10.5194/wcd-5-959-2024, 2024.

Foudad, M., Sanchez-Gomez, E., Jaravel, T., Rochoux, M. C., and Terray, L.: Past and future trends in clear-air turbulence over the northern hemisphere, Journal of Geophysical Research: Atmospheres, 129, 2024.

Gratton, G. B., Williams, P. D., Padhra, A., and Rapsomanikis, S.: Reviewing the impacts of climate change on air transport operations, The Aeronautical Journal, 126, 209–221, 2022.

Guarino, M.-V., Teixeira, M. A., Keller, T. L., and Sharman, R. D.: Mountain-wave turbulence in the presence of directional wind shear over the Rocky Mountains, Journal of the Atmospheric Sciences, 75, 1285–1305, 2018.

Hersbach, H., Bell, B., Berrisford, P., Hirahara, S., Horányi, A., Muñoz-Sabater, J., Nicolas, J., Peubey, C., Radu, R., Schepers, D., et al.: The ERA5 global reanalysis, Quarterly journal of the royal meteorological society, 146, 1999–2049, 2020.

(ICAO), I. C. A. O.: Seventh Meeting of the MOG, https://www.icao.int/airnavigation/METP/Seventh%20Meeting%20of%20the%20MOG/METPWGMOG-7_Attachment_SN_35_METP_4_WP.xxxx.Revised_EDR_values_Amd_79_vs_1.0_22mar2018.docx, accessed: 2024-07-12, 2018.

Jaeger, E. B. and Sprenger, M.: A Northern Hemispheric climatology of indices for clear air turbulence in the tropopause region derived from ERA40 reanalysis data, Journal of Geophysical Research: Atmospheres, 112, 2007.

Jézéquel, A., Dépoues, V., Guillemot, H., Trolliet, M., Vanderlinden, J.-P., and Yiou, P.: Behind the veil of extreme event attribution, Climatic Change, https://doi.org/10.1007/s10584-018-2252-9, 2018.

Kaluza, T., Williams, P. D., Schultz, D. M., and Banyard, T. P.: Climatology of upper-tropospheric turbulence: capabilities and limitations of aircraft reports and ERA5 reanalysis diagnostics, Quarterly Journal of the Royal Meteorological Society, 152, e70 073, 2026.

Keel, T., Brierley, C., Edwards, T., and Frame, T. H. A.: Exploring Uncertainty of Trends in the North Pacific Jet Position, Geophysical Research Letters, 51, e2024GL109 500, https://doi.org/10.1029/2024GL109500, 2024.

Kim, J.-H. and Chun, H.-Y.: A Numerical Study of Clear-Air Turbulence Encounters over South Korea on 2 April 2007, Journal of Applied Meteorology and Climatology, 49, 2381–2403, 2010.

Kim, J.-H. and Chun, H.-Y.: A Numerical Simulation of Convectively Induced Turbulence above Deep Convection, Journal of Applied Meteorology and Climatology, 51, 1180–1200, 2012.

Kim, J.-H., Chun, H.-Y., Sharman, R. D., and Trier, S. B.: The Role of Vertical Shear on Aviation Turbulence within Cirrus Bands of a Simulated Western Pacific Cyclone, Monthly Weather Review, 142, 2794–2813, 2014.

Kim, S.-H., Chun, H.-Y., Kim, J.-H., Sharman, R. D., and Strahan, M.: Retrieval of Eddy Dissipation Rate from Derived Equivalent Vertical Gust Included in Aircraft Meteorological Data Relay (AMDAR), Atmospheric Measurement Techniques, 13, 1373–1385, https://doi.org/10.5194/amt-13-1373-2020, 2020.

Kim, S.-H., Chun, H.-Y., Lee, D.-B., Kim, J.-H., and Sharman, R. D.: Improving Numerical Weather Prediction-Based Near-Cloud Aviation Turbulence Forecasts by Diagnosing Convective Gravity Wave Breaking, Weather and Forecasting, 36, 1735–1757, 2021.

Lane, T. P., Sharman, R. D., Trier, S. B., Fovell, R. G., and Williams, J. K.: Recent Advances in the Understanding of Near-Cloud Turbulence, Bulletin of the American Meteorological Society, 93, 499 – 515, https://doi.org/10.1175/BAMS-D-11-00062.1, 2012.

Lee, J. H., Kim, J.-H., Sharman, R. D., Kim, J., and Son, S.-W.: Climatology of Clear-Air Turbulence in Upper Troposphere and Lower Stratosphere in the Northern Hemisphere Using ERA5 Reanalysis Data, Journal of Geophysical Research: Atmospheres, 128, e2022JD037 679, https://doi.org/https://doi.org/10.1029/2022JD037679, e2022JD037679 2022JD037679, 2023.

Lee, J. H., Kim, J.-H., Trier, S. B., Sharman, R. D., and Doyle, J. D.: Generation Mechanisms of Near-Cloud Turbulence Events in the Upper-Level Outflow of Tropical Cyclone Hagibis, Monthly Weather Review, 153, 521–542, https://doi.org/10.1175/MWR-D-24-0116.1, 2025.

Prosser, M. C., Williams, P. D., Marlton, G. J., and Harrison, R. G.: Evidence for Large Increases in Clear-Air Turbulence Over the Past Four Decades, Geophys. Res. Lett., 50, e2023GL103814, https://doi.org/10.1029/2023GL103814, 2023.

Rapella, L., Alberti, T., Faranda, D., and Drobinski, P.: Anthropogenic climate change has increased severity of mid-latitude storms and impacted airport operations, Weather and Climate Dynamics, 6, 1339–1363, https://doi.org/10.5194/wcd-6-1339-2025, 2025.

Sharman, R. and Lane, T.: Aviation turbulence, Springer International Publishing, Switzerland, DOI, 10, 978–3, 2016.

Sharman, R., Cornman, L., Meymaris, G., Pearson, J., and Farrar, T.: Description and derived climatologies of automated in situ eddy-dissipation-rate reports of atmospheric turbulence, Journal of applied meteorology and climatology, 53, 1416–1432, 2014.

Shaw, T. A. and Miyawaki, O.: Fast upper-level jet stream winds get faster under climate change, Nature Climate Change, https://doi.org/10.1038/s41558-023-01884-1, 2023.

Smith, I. H., Williams, P. D., and Schiemann, R.: Clear-air turbulence trends over the North Atlantic in high-resolution climate models, Climate Dynamics, pp. 1–17, 2023.

Storer, L. N., Williams, P. D., and Joshi, M. M.: Global response of clear-air turbulence to climate change, Geophysical Research Letters, 44, 9976–9984, 2017.

Storer, L. N., Williams, P. D., and Gill, P. G.: Aviation turbulence: dynamics, forecasting, and response to climate change, Pure and Applied Geophysics, 176, 2081–2095, 2019.

Trier, S. B., Sharman, R. D., Muñoz-Esparza, D., and Lane, T. P.: Environment and Mechanisms of Severe Turbulence in a Midlatitude Cyclone, Journal of the Atmospheric Sciences, 77, 3869–3889, https://doi.org/10.1175/JAS-D-20-0095.1, 2020.

Williams, P. D.: Increased light, moderate, and severe clear-air turbulence in response to climate change, Advances in Atmospheric Sciences, 34, 576–586, 2017.

Williams, P. D. and Joshi, M. M.: Intensification of winter transatlantic aviation turbulence in response to climate change, Nature Climate Change, 3, 644–648, https://doi.org/10.1038/nclimate1866, 2013.

Yiou, P., Jézéquel, A., Naveau, P., Otto, F. E. L., Vautard, R., and Vrac, M.: A statistical framework for conditional extreme event attribution, Advances in Statistical Climatology, Meteorology and Oceanography, 3, 17–31, https://doi.org/10.5194/ascmo-3-17-2017, 2017.